8
Regge cuts

8.1 Introduction

In section 4.8 we demonstrated that the occurrence of Gribov–Pomeranchuk fixed poles at wrong-signature nonsense points, generated by the third double spectral function, ρ_{su}, requires that there be cuts in the t-channel angular-momentum plane. Otherwise it is impossible to satisfy t-channel unitarity. We have also found in section 6.8 that, despite the many successes of Regge pole phenomenology, there are some features of the data that poles alone cannot explain. These are mainly failures of factorization, and it seems natural to try an invoke Regge cuts, which correspond to the exchange of two or more Reggeons and so are not expected to factorize, to make good these defects.

Unfortunately we still have a much less complete understanding of the properties of Regge cuts than of the properties of poles. On the phenomenological side, this is mainly because it is difficult to be sure whether cuts or poles are responsible for what is observed, since the main tests, $\log s$ behaviour (see (8.5.12) below) and lack of factorization, are hard to apply. Though cuts do not have to factorize some models suggest that they do, at least approximately. We shall review some of these problems in section 8.7.

Also the various theoretical models which have been used to gain insight into the behaviour of Regge poles (discussed in chapter 3) are harder to apply to cuts. For example in potential scattering, which has only elastic unitarity and no third double spectral function, there are no Regge cuts if the potentials are well behaved. Though if the potential is singular, say

$$U(r) = \frac{V_0}{r^2} + \overline{V}(r) \tag{8.1.1}$$

where $\overline{V}(r)$ is regular as $r \to 0$, the radial Schroedinger equation becomes

$$\frac{\mathrm{d}^2\phi_l(r)}{\mathrm{d}r^2} + \left[k^2 - \frac{l(l+1)+V_0}{r^2} - \overline{V}(r)\right]\phi_l(r) = 0 \tag{8.1.2}$$

which has the same form as (3.3.3) if l is replaced by L, where

$$L(L+1) \equiv l(l+1) + V_0 \tag{8.1.3}$$

https://doi.org/10.1017/9781009403269.009 Published online by Cambridge University Press

so the solutions will be meromorphic in L. But a pole at $L = \alpha$ gives, on inverting (8.1.3), branch points in the l plane at

$$l = \tfrac{1}{2}\{-1 \pm [1 - 4V_0 + 4\alpha(\alpha+1)]^{\frac{1}{2}}\} \tag{8.1.4}$$

so the singular part of the potential produces cuts in the l plane. But there is no reason to suppose that similar cuts will occur in strong interactions, because they do not seem to be related to multi-Reggeon exchange.

Instead it is necessary to rely mainly on Feynman-diagram models to deduce the properties of Regge cuts. But, as we shall find in the next section, there are difficulties associated with the many-to-one correspondence between Feynman diagrams and unitarity diagrams and the convergence of the perturbation series, which limit the applicability of these models in strong interactions. Gribov (1968) has developed an ingenious scheme for inserting Regge poles themselves into Feynman diagrams, giving a 'Reggeon calculus' from which one can deduce the discontinuities across J-plane cuts, analogous to the unitarity diagram approach to s-plane discontinuities. This calculus, to be discussed in section 8.3, has allowed considerable progress though the theory is still incomplete.

We shall also examine some popular approximation methods for calculating cut contributions, in particular the absorption and eikonal models, before going on to examine the phenomenological application of these ideas in the final section. Much of the discussion is rather technical and the reader is advised to skip the more difficult parts at the first reading. If he is mainly interested in phenomenology he could go straight to section 8.7 and refer back as necessary.

8.2 Regge cuts and Feynman diagrams*

We found in section 3.4 that a single Regge pole exchange corresponds to the set of ladder Feynman diagrams like fig. 8.1, where we sum over all possible numbers of rungs as in (3.4.12). Regge cuts arise from the exchange of two (or more) Reggeons, and so the simplest type of diagram which might be expected to produce a Regge cut is fig. 8.2. This is a planar diagram, and the rules for obtaining the asymptotic behaviour of such diagrams are comparatively simple, because they depend only on the 'end-point' contributions (see section 3.4).

The asymptotic power behaviour of a ladder diagram as

* This section may be omitted at first reading.

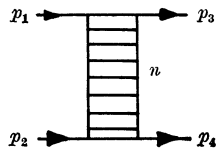

FIG. 8.1 A ladder Feynman diagram which contributes to a t-channel Regge pole.

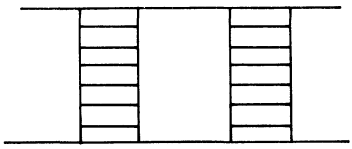

FIG. 8.2 A two-ladder diagram which might be expected to produce a Regge cut.

$s = (p_1+p_2)^2 \to \infty$, $t = (p_1-p_3)^2$ fixed, is s^{-1} (from (3.4.11)), independent of the number of rungs because just one propagator is needed to cross the diagram; and the leading s behaviour is $s^{-1}(\log s)^{n-1}$ because there are n different independent paths by which one might cross the diagram. This result can be generalized for (most) planar diagrams as follows (Eden *et al.* (1966) p. 138).

We look for paths through the graph (i.e. connected sets of internal lines) which if short-circuited split the graph into two parts which have only a single vertex and no lines in common, p_1 and p_3 being coupled to one side, and p_2 and p_4 to the other (assuming we are considering $s \to \infty$, t fixed). The three different ways of doing this for fig. 8.3 (a) are shown in figs. 8.3 (b), (c), (d). We select those paths which are of the minimum length, i.e. those which involve short-circuiting the smallest number of lines. Thus figs. 8.3 (c) and (d) are included because they short-circuit only two lines, but fig. 8.3 (b) which involves three lines is excluded. These paths of minimum length are called 'd-lines'. The rule is that the asymptotic power of s for a diagram whose d-lines are of length m is s^{-m}. So fig. 8.3 (a) with d-lines of length 2 behaves like $\sim s^{-2}$, while the ladder fig. 8.1, with d-lines of length 1, $\sim s^{-1}$.

If there are n such d-lines (all of the same minimum length m) for a given diagram, then the asymptotic behaviour will be

$$\sim s^{-m}(\log s)^{n-1}, \quad m, n \geqslant 1 \tag{8.2.1}$$

Thus since fig. 8.3 (a) has 2 d-lines its behaviour is $\sim s^{-2}\log s$. This rule obviously also works for ladder diagrams to give (3.4.11). Some graphs, involving 'singular configurations', are exceptions to these rules (see Eden *et al.* p. 141) but we shall not need to consider them here.

If we apply (8.2.1) to the two-ladder graph (fig. 8.2) we see that its d-lines are the two paths across the top and bottom of the diagram, each of length 3, and so $m = 3$, $n = 2$. Thus all diagrams like fig. 8.2

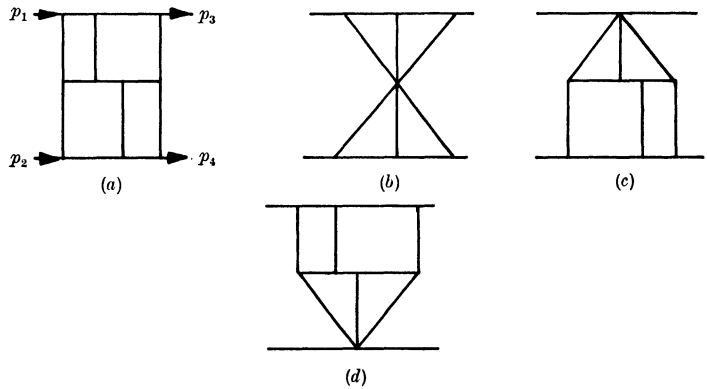

FIG. 8.3 (*a*) A Feynman diagram; and (*b*), (*c*) and (*d*) the three ways of short-circuiting it, as described in the text.

behave like $s^{-3}\log s$ independent of the number of rungs in the two ladders. So the sum of all such diagrams, with all possible numbers of rungs, may be expected also to have this behaviour (provided the sum converges), and so to give rise to a fixed singularity at $l = -3$ (see (2.7.4)), not a moving Regge cut.

Regge behaviour stems from summing over all powers of $\log s$ in (3.4.12), and it is the fact that only the first power of $\log s$ occurs in the leading asymptotic behaviour of all the diagrams like fig. 8.2 which prevents Reggeization. If we sum sets of such diagrams, like fig. 8.4, the sum would give us a Regge pole like (3.4.12) but with $\alpha(\infty) = -3$. The small ladders simply give re-normalizations of the basic ladder diagram fig. 8.1. This shows why planar diagrams, whose asymptotic behaviour comes just from end-point singularities, contribute only to the Regge poles, not to the cuts.

However, if we take the discontinuity of fig. 8.2 across the two-particle intermediate state, as shown in fig. 8.5(*a*), the two-body unitarity condition (1.5.7) gives the two particle discontinuity

$$\frac{1}{2i}(A^+ - A^-) \equiv \Delta_2\{A(s,t)\} = \frac{q_s}{32\pi^2\sqrt{s}}\int A^1(s,t_1)\,A^{2*}(s,t_2)\,\mathrm{d}\Omega_s \tag{8.2.2}$$

where $\mathrm{d}\Omega_s$ is the element of solid angle in the intermediate state (see fig. 2.1) and $A^1(s,t_1)$ and $A^2(s,t_2)$ are the ladder amplitudes shown in the figure. If this equation is decomposed into s-channel partial waves we get (see (2.2.7))

$$\Delta_2\{A_l(s)\} = \frac{2q_s}{\sqrt{s}}A^1_l(s)A^{2*}_l(s) \tag{8.2.3}$$

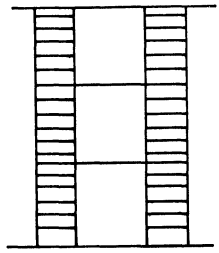

FIG. 8.4 A 'ladder of ladders' diagram which contributes to the re-normalization of the simple 4-rung ladder diagram.

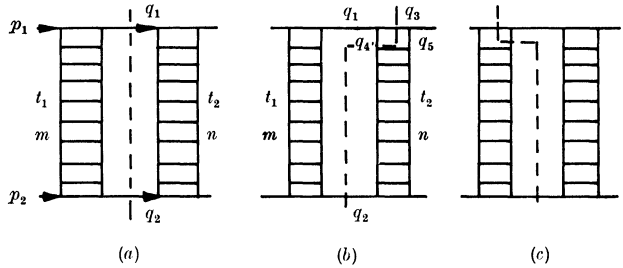

FIG. 8.5 (*a*) Fig. 8.2 cut across the two-body intermediate state; (*b*) a cut across a three-body state; (*c*) a similar cut.

where $$A_l^1(s) = \frac{1}{32\pi}\int_{-1}^{1} A^1(s,t_1)\,P_l(z_1)\,\mathrm{d}z_1, \quad z_1 \equiv z_s(s,t_1) \tag{8.2.4}$$

etc., and so on summing the partial-wave series (2.2.2),

$$\begin{aligned}\Delta_2\{A(s,t)\} &= 16\pi\sum_l (2l+1)\,P_l(z_s)\,\Delta_2\{A_l(s)\}\\ &= 16\pi\sum_l (2l+1)\,P_l(z_s)\frac{2q_s}{\sqrt{s}}\frac{1}{32\pi}\int_{-1}^{1} A^1(s,t_1)\,P_l(z_1)\,\mathrm{d}z_1\\ &\quad\times\frac{1}{32\pi}\int_{-1}^{1} A^{2*}(s,t_2)\,P_l(z_2)\,\mathrm{d}z_2\end{aligned} \tag{8.2.5}$$

But (Goldberger and Watson (1964) p. 595; Henyey *et al.* (1969))

$$\sum_l (2l+1)\,P_l(z_s)\,P_l(z_1)\,P_l(z_2) = \frac{2}{\pi}\frac{\theta(\Delta)}{\Delta^{\frac{1}{2}}} \tag{8.2.6}$$

where $$\Delta \equiv 1 - z_s^2 - z_1^2 - z_2^2 + 2z_s z_1 z_2 \tag{8.2.7}$$

and $\theta(\Delta)$ is the step function

$$\theta(\Delta) = 0, \quad \Delta < 0; \quad \theta(\Delta) = 1, \quad \Delta > 0 \tag{8.2.8}$$

https://doi.org/10.1017/9781009403269.009 Published online by Cambridge University Press

and so

$$\Delta_2\{A(s,t)\} = \frac{g_s}{16\pi^2\sqrt{s}}\int_{-1}^{1} dz_1 \int_{-1}^{1} dz_2 A^1(s,t_1)\, A^{2*}(s,t_2)\frac{\theta(\Delta)}{\Delta^{\frac{1}{2}}} \tag{8.2.9}$$

Then for large s and small t, from (1.7.22),

$$z_1 \approx 1+\frac{2t_1}{s}, \quad z_2 \approx 1+\frac{2t_2}{s}, \quad z_s \approx 1+\frac{2t}{s} \tag{8.2.10}$$

so (8.2.9) becomes

$$\Delta_2\{A(s,t)\} \approx \frac{1}{16\pi^2 s}\int_{-\infty}^{0} dt_1 \int_{-\infty}^{0} dt_2 A^1(s,t_1)\, A^{2*}(s,t_2)\, \frac{\theta(-\lambda)}{(-\lambda(t,t_1,t_2))^{\frac{1}{2}}} \tag{8.2.11}$$

where $$\lambda(t,t_1,t_2) \equiv t^2+t_1^2+t_2^2-2(tt_1+tt_2+t_1t_2) \tag{8.2.12}$$

(see (1.7.11)). The result, from (1.5.3)–(1.5.7) and (8.2.2)–(8.2.11), that for $s\to\infty$, t small,

$$\int \frac{d^4q}{(2\pi)^4} 2\pi\,\delta((p_1+q)^2-m^2)\, 2\pi\,\delta((p_2-q)^2-m^2)$$
$$\to \int \frac{d^2\mathbf{q}_\perp}{(2\pi)^2} \to \frac{1}{8\pi^2|s|}\int_{-\infty}^{0}\int_{-\infty}^{0} dt_1\, dt_2 \frac{\theta(-\lambda)}{(-\lambda)^{\frac{1}{2}}} \tag{8.2.13}$$

will frequently be of use for phase-space integrations in the high energy limit.

So if, for example, we represent each ladder sum by a linear Regge pole amplitude

$$A^i(s,t) \sim s^{\alpha_i(t)} = e^{(\alpha_i{}^0+\alpha_i' t)\log s} \tag{8.2.14}$$

since it is found that (O'Donovan 1969)

$$\int_{-\infty}^{0} dt_1 \int_{-\infty}^{0} dt_2\, e^{(b_1t_1+b_2t_2)}\frac{\theta(-\lambda)}{(-\lambda)^{\frac{1}{2}}} = \pi\frac{e^{[b_1b_2/(b_1+b_2)]t}}{b_1+b_2} \tag{8.2.15}$$

(8.2.11) gives, for $\log s\to\infty$,

$$\Delta_2\{A(s,t)\} \sim \frac{s^{(\alpha_1{}^0+\alpha_2{}^0-1)+[\alpha_1'\alpha_2'/(\alpha_1'+\alpha_2')]t}}{(\alpha_1'+\alpha_2')\log s} \tag{8.2.16}$$

which corresponds to a Regge cut at

$$\alpha_c(t) = \alpha_1^0+\alpha_2^0-1+\left(\frac{\alpha_1'\alpha_2'}{\alpha_1'+\alpha_2'}\right)t \tag{8.2.17}$$

with a finite discontinuity at the branch point (see (2.7.4)). As long as the trajectories $\alpha_i(t_i)$ are monotonically increasing functions of t_i in $-\infty < t_i < 0$, the leading behaviour of (8.2.11) will come from the region $\lambda = 0$, which from (8.2.12) implies (since $t_1, t_2, t \leqslant 0$)

$$\sqrt{-t} = \sqrt{-t_1}+\sqrt{-t_2} \tag{8.2.18}$$

https://doi.org/10.1017/9781009403269.009 Published online by Cambridge University Press

so more generally $$\alpha_c(t) = \max\{\alpha_1(t_1) + \alpha_2(t_2) - 1\} \tag{8.2.19}$$

subject to (8.2.18). The reader can easily check that (8.2.19) gives (8.2.17) for linear trajectories.

This argument mistakenly led Amati, Fubini and Stanghellini (1962) to suppose that fig. 8.2 would give rise to a Regge cut (now called an AFS cut). However, we know that the asymptotic behaviour of the diagram is actually $s^{-3}\log s$ not (8.2.16), so this Regge cut behaviour of the two-particle discontinuity must be cancelled by the other discontinuities of fig. 8.2, such as fig. 8.5 (*b*) (Mandelstam 1963). This cancellation has been demonstrated nicely by Halliday and Sachrajda (1973).

The discontinuity across the two-particle cut fig. 8.5 (*a*) may be written

$$\Delta_2\{A\} = \tfrac{1}{2}\iint \frac{\mathrm{d}^4q_1}{(2\pi)^4}\frac{\mathrm{d}^4q_2}{(2\pi)^4}(2\pi)\,\delta(q_1^2-m^2)\,(2\pi)\,\delta(q_2^2-m^2) \times (2\pi)^4\,\delta^4(q_1+q_2-p_1-p_2)\,A_m A_n^* \tag{8.2.20}$$

As usual $$s = (p_1+p_2)^2, \quad t = (p_1-p_3)^2 = q^2 \tag{8.2.21}$$

and we introduce the four-vectors

$$p_1' = p_1 - \frac{m^2}{s}p_2, \quad p_2' = p_2 - \frac{m^2}{s}p_1 \tag{8.2.22}$$

which have the property that (using (1.7.4))

$$p_1'^2 = p_2'^2 = 0 + O\left(\frac{1}{s^2}\right) \quad \text{and} \quad 2p_1'.p_2' = s \tag{8.2.23}$$

Then introducing Sudakov variables α_i, β_i and $\boldsymbol{q}_{i\perp}$ for each four-vector q_i (see Halliday and Saunders 1968)

$$q_i = \alpha_i p_1' + \beta_i p_2' + \boldsymbol{q}_{i\perp}, \quad i = 1, 2 \tag{8.2.24}$$

where $\boldsymbol{q}_{i\perp}$ is a two-vector perpendicular to the plane containing p_1' and p_2', and α_i and β_i give the components of q_i in the directions of p_2' and p_1', respectively. Thus we have

$$\mathrm{d}^4q_i\,\delta(q_i^2-m_i^2) = \tfrac{1}{2}|s|\,\mathrm{d}\alpha_i\,d\beta_i\,\mathrm{d}^2\boldsymbol{q}_{i\perp}\,\delta(\alpha_i\beta_i s-\mu_i^2) \tag{8.2.25}$$

where $$\mu_i^2 \equiv m^2 + \boldsymbol{q}_{i\perp}^2 \tag{8.2.26}$$

and $$\delta^4(p_1+p_2-\Sigma q_i) = \delta(\Sigma\alpha_i - 1)\,\delta(\Sigma\beta_i - 1)\,\delta(\Sigma\boldsymbol{q}_{i\perp})\frac{2}{|s|} \tag{8.2.27}$$

and so

$$\Delta_2\{A\} = \frac{1}{(2\pi)^2}\int \frac{\mathrm{d}\alpha_1\,\mathrm{d}\beta_1}{2\alpha_1\,2\beta_2}\,\delta(\alpha_1+\alpha_2-1)\,\delta(\beta_1+\beta_2-1)\,A_m A_n^* \times \mathrm{d}^2\boldsymbol{q}_{1\perp}\,\mathrm{d}^2\boldsymbol{q}_{2\perp}\,\delta(\boldsymbol{q}_{1\perp}+\boldsymbol{q}_{2\perp}) \tag{8.2.28}$$

https://doi.org/10.1017/9781009403269.009 Published online by Cambridge University Press

The momentum transfer down the left-hand ladder is

$$t_1 = (p_1 - q_1)^2 \to (\alpha_1 - 1)\beta_1 s - \boldsymbol{q}_\perp^2 \tag{8.2.29}$$

which must remain finite as $s \to \infty$ if we are to remain in the Regge regime, so as $s \to \infty$ we are interested in the integration region $\beta_1 \sim 1/s$, $\alpha_1 \sim$ constant, and so from the δ functions in (8.2.28) we must have $\beta_2 \sim 1$, $\alpha_2 \sim 1/s$, $\alpha_1 \sim 1$. So as $s \to \infty$

$$\Delta_2\{A\} = \frac{1}{16\pi^2 s}\int A_m A_n^* \, \mathrm{d}^2\boldsymbol{q}_{1\perp} \tag{8.2.30}$$

Then if we insert (3.4.11) for the asymptotic behaviour of the ladder diagrams we get

$$\Delta_2\{A\} = \frac{g^4}{16\pi^2 s^3}\frac{(\log s)^{m+n-2}}{(m-1)!\,(n-1)!}\int K(t_1)^{m-1} K(t_2)^{n-1} \, \mathrm{d}^2\boldsymbol{q}_{1\perp} \tag{8.2.31}$$

which is just the result needed to obtain (8.2.16) after summation over all numbers of rungs.

But if we consider the discontinuity of fig. 8.5(*b*), the left-hand side has

$$A^{\mathrm{L}} = A_m \frac{g}{q_1^2 - m^2}$$

and the right-hand side has one rung subtracted so

$$A^{\mathrm{R}} = A_{n-1}\frac{g}{q_5^2 - m^2}$$

and it is found after integration over q_2, q_3 and q_4 that

$$\Delta_3\{A\} = -\frac{g^4}{16\pi^2 s^3}\frac{(\log s)^{m+n-2}}{(m+n-2)!\,(m-1)!\,(n-2)!}\int K(t_1)^{m-1} K(t_2)^{n-1} \, \mathrm{d}^2\boldsymbol{q}_{1\perp} \tag{8.2.32}$$

Then adding fig. 8.5(*c*) which is the same with $m \leftrightarrow n$ we get an exact cancellation of the leading behaviour of fig. 8.5(*a*), i.e. (8.2.31). Similarly there is a cancellation among the leading behaviours of all the other possible unitary dissections of fig. 8.2, and so no Regge cut actually appears. (In fact the AFS cut occurs on the unphysical sheet reached through the two-body cut in s.)

The above is a very good example of the dangers which lurk in the many-to-one correspondence between Feynman and unitarity diagrams.

To obtain a Regge cut we must look at non-planar diagrams in

https://doi.org/10.1017/9781009403269.009 Published online by Cambridge University Press

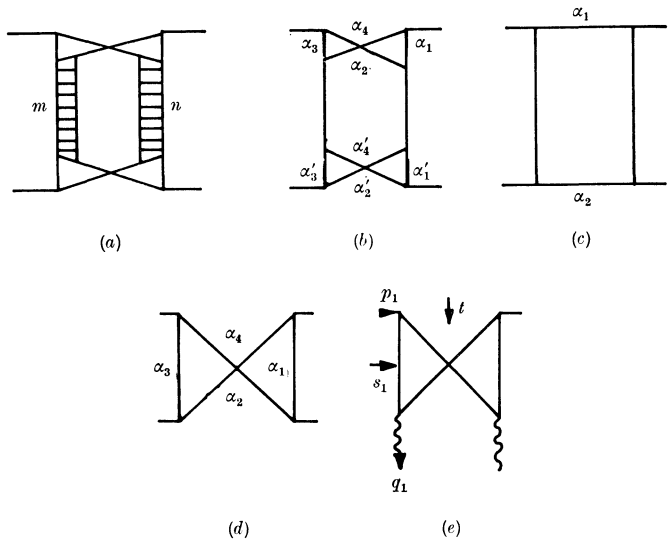

Fig. 8.6 (*a*) Mandelstam's double-cross diagram. (*b*) The most elementary form of (*a*) with the Feynman parameters. (*c*) The box diagram which does not have a 'pinch' asymptotic behaviour. (*d*) The cross diagram. (*e*) The cross diagram in particle–Reggeon scattering.

which the leading behaviour comes from the pinching of singularities (Eden *et al.* p. 158). The simplest such diagram is Mandelstam's 'double-cross' diagram, fig. 8.6(*a*), of which the simplest form is fig. 8.6(*b*). This has 6 d-lines each of length 2 and so the end-point behaviour is $\sim s^{-2}(\log s)^5$. However we have seen that the cross is the simplest diagram which can produce a Gribov–Pomeranchuk fixed pole at $l = -1$ in the t-channel angular-momentum plane (see (2.8.7)), so it should have an $\sim s^{-1}$ behaviour.

The coefficient of s in the Feynman denominator of (3.4.4) is

$$(\alpha_1\alpha_3 - \alpha_2\alpha_4)(\alpha'_1\alpha'_3 - \alpha'_2\alpha'_4) \equiv x_1x_2 \quad \text{(say)} \tag{8.2.33}$$

and when we integrate over the α's $(0 \to 1)$ there will be points where both brackets x_1 and x_2 vanish. In this region the integral takes the form

$$\int_{a_1}^{b_1} \mathrm{d}x_1 \int_{a_2}^{b_2} \mathrm{d}x_2 \frac{1}{(x_1x_2s+d)^2} = -\frac{1}{sd}\log\left[\frac{(a_1a_2s+d)(b_1b_2s+d)}{(a_1b_2s+d)(a_2b_1s+d)}\right] + \ldots \tag{8.2.34}$$

Now as s tends to ∞ the argument of the log tends to 1, and as $\log 1 = 0$ we get the expected s^{-2} behaviour, but only if all a_i, $b_i > 0$ or all

https://doi.org/10.1017/9781009403269.009 Published online by Cambridge University Press

$a_i, b_i < 0$. If say $a_1, a_2 < 0$ and $b_1, b_2 > 0$ then as s tends to ∞ the numerator in the log tends to $\infty + i\epsilon$ while the denominator tends to $\infty - i\epsilon$, so the log tends to $2\pi i$ giving instead (8.2.34) $\sim -2\pi i(sd)^{-1}$. So the vanishing of the brackets in (8.2.33) gives a pinch asymptotic behaviour which is different from that of the end-point singularities. In the box diagram fig. 8.6 (*c*) x_1 and x_2 are replaced by α_1 and α_2 respectively which vanish only at the end-points.

If we now return to fig. 8.6 (*a*) the leading singularity comes from the pinch singularities of the crosses, together with the end-point singularities of the ladders, (3.4.11), and the asymptotic behaviour is found to be

$$\frac{ig^4}{16\pi^2}\int dt_1 \int dt_2 \frac{(N(t,t_1,t_2))^2\,\theta(-\lambda)}{(-\lambda(t,t_1,t_2))^{\frac{1}{2}}} \frac{K(t_1)^{m-1}K(t_2)^{n-1}(\log s)^{m+n-2}}{(m-1)!\,(n-1)!\,s^3} \tag{8.2.35}$$

where $K(t)$ is the box diagram function (3.4.9), and N is the Feynman integral of the cross diagram fig. 8.6 (*d*) in the pinch configuration, i.e.

$$N = \int_0^1 d\alpha_1 \ldots d\alpha_4 \frac{\delta(\Sigma\alpha - 1)\,\delta(\alpha_1\alpha_3 - \alpha_2\alpha_4)}{d(t,t_1,t_2,\alpha)} \tag{8.2.36}$$

d being its Feynman denominator. N appears squared because fig. 8.6 (*a*) contains two identical crosses. Then if we sum (8.2.35) over all possible numbers of rungs in the ladders we get

$$A = \frac{ig^4}{16\pi^2}\int dt_1 \int dt_2 \frac{(N(t,t_1,t_2))^2\,\theta(-\lambda)}{(-\lambda(t,t_1,t_2))^{\frac{1}{2}}} s^{\alpha(t_1)+\alpha(t_2)-1} \tag{8.2.37}$$

$$\alpha(t) = -1 + K(t)$$

which agrees with AFS result (8.2.19) for the position of the cut, and gives (8.2.17) if the trajectories are linear.

So the Mandelstam diagram, fig. 8.6 (*a*), produces a branch point whose location in the l plane is identical to that of the AFS cut, fig. 8.5 (*a*). But (8.2.37) differs from (8.2.11) not only through the occurrence of N^2, but because (8.2.11) involves A_n^* where as (8.2.35) does not. (Equation (8.2.11) has been divided by 2i because we have taken the discontinuity.) And whereas the AFS cut occurs only on unphysical sheets, the Mandelstam cut is present on the physical sheet and so contributes to the asymptotic behaviour.

Another way of seeing why the non-planar structure is necessary is to note that we can write

$$N(t,t_1,t_2) = \int_{-\infty}^{\infty} ds_1 A_1(s_1,t,t_1,t_2) \tag{8.2.38}$$

https://doi.org/10.1017/9781009403269.009 Published online by Cambridge University Press

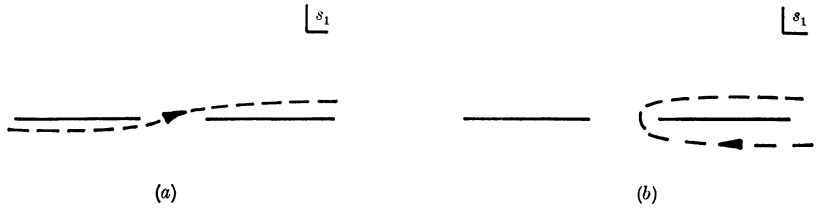

FIG. 8.7 (*a*) Integration contour along the real s_1 axis.
(*b*) Deformed contour round the positive s_1 cuts.

where $A_1(s_1, t, t_1, t_2)$ is the Reggeon–particle scattering amplitude for the cross (fig. 8.6 (*e*)), and $s_1 = (p_1 - q_1)^2$, the integration contour being as in fig. 8.7 (*a*). Since $A_1 \sim s^{-2}$ we can close the contour at infinity as in fig. 8.7 (*b*) and obtain

$$N(t, t_1, t_2) = 2\mathrm{i} \int_{4m^2}^{\infty} \mathrm{Im}\{A_1(s_1, t, t_1, t_2)\}\, \mathrm{d}s_1 \qquad (8.2.39)$$

which is just the residue of the Gribov–Pomeranchuk fixed pole in A_1, i.e. in (4.8.4) at $J_0 = -1$, $\lambda = \lambda' = 0$. However, if the amplitude did not have the cross-structure, and hence only had singularities for positive s_1, we should be able to close the contour in the upper half-plane, and so find $N = 0$, which is what happens in the AFS case. The contribution of the pole at $q_1^2 = s = m^2$ in fig. 8.5 (*a*) is cancelled by the right-hand cut due to the singularities of the vertex function coupling this particle to the Reggeon, the simplest contributions to which are the lines q_3 and q_4 in fig. 8.5 (*b*) – see Rothe (1967), Landshoff and Polkinghorne (1971).

A rather more physical understanding of this result can be obtained by considering scattering of composite particles, say deuterons. In d–d scattering, in addition to the single exchange diagram fig. 8.8 (*a*), there are various double scattering diagrams, figs. 8.8 (*b*), (*c*). Of these fig. 8.8 (*b*) becomes very improbable at high energies because it requires a given pair of nucleons to scatter off each other twice, despite the fact that they are passing each other very rapidly. On the other hand fig. 8.8 (*c*), which involves each nucleon in only a single scattering, can perfectly well occur even at very high energies. So the planar diagram (*b*) dies away at high energies, but (*c*), which depends in an essential way on the deuterons being composite, remains. Obviously (*c*) has the same structure as the Mandelstam diagram, fig. 8.6 (*a*). (The connection between Regge cuts and Glauber's multiple scattering theory is complicated, however; see Glauber (1959), Abers *et al.* (1966), Harrington (1970).)

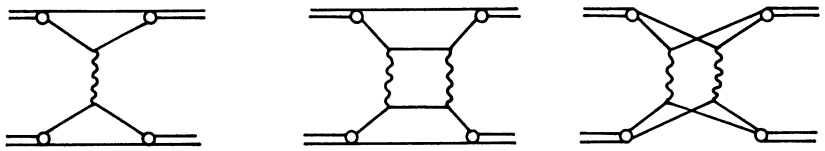

(*a*) (*b*) (*c*)

FIG. 8.8 Deuteron–deuteron scattering. (*a*) Single interaction between one pair of nucleons. (*b*) Double interaction between a pair of nucleons. (*c*) Double interaction between different pairs of nucleons.

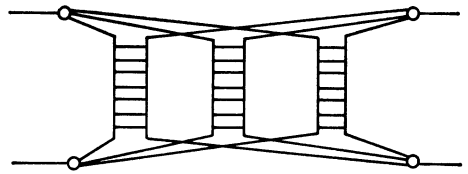

FIG. 8.9 A three-Reggeon cut diagram.

A three-ladder diagram, with non-planar couplings between each as in fig. 8.9, gives rise to a three-Reggeon cut, and so on.

The above discussion should be sufficient to demonstrate that cuts are much more difficult to deal with than poles because, quite apart from the technical difficulties (which we have skated over in this brief account), to calculate the magnitude of the cut contribution one has to make use of the off-mass-shell properties of the Feynman integrals, and not just the discontinuities of the integrals for which the particles are on the mass shell. Hence we are left with the function $N(t, t_1, t_2)$ which is known only as a Feynman integral, not as a physical quantity.

A somewhat more systematic way of analysing these problems has been invented by Gribov: the Reggeon calculus.

8.3 The Reggeon calculus*

The Reggeon calculus (Gribov 1968) uses Feynman integrals for the couplings of the Reggeons, but replaces the ladders directly by Regge poles. The plausibility of doing this depends on results such as (8.2.37).

Thus the Mandelstam diagram fig. 8.5 is replaced directly by fig. 8.10 where R_1 and R_2 are Regge poles. There are then just three closed loops, two corresponding to the crosses, plus the loop including

* This section may be omitted at first reading.

https://doi.org/10.1017/9781009403269.009 Published online by Cambridge University Press

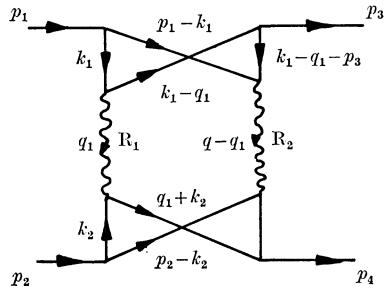

FIG. 8.10 Two-Reggeon cut diagram. $q_2 \equiv q-q_1$, $q \equiv p_1-p_3$.

the Reggeons, so the Feynman rules give

$$A^{c}(s,t) = \frac{ig^4}{2}\int \frac{d^4q_1}{(2\pi)^4}\frac{d^4k_1}{(2\pi)^4}\frac{d^4k_2}{(2\pi)^4}\frac{A^{R_1}(q_1,k_1,k_2)\,A^{R_2}(q-q_1,p_1-k_1,p_2-k_2)}{\prod_{m=1}^{8} d_m} \tag{8.3.1}$$

where the d's are the Feynman propagators

$$\left.\begin{aligned} d_1 &= k_1^2-m^2+i\epsilon \\ d_2 &= (p_1-k_1)^2-m^2+i\epsilon, \quad \text{etc.} \end{aligned}\right\} \tag{8.3.2}$$

If we introduce Sudakov variables like (8.2.24)

$$\left.\begin{aligned} q_1 &= \alpha p_2' + \beta p_1' + \boldsymbol{q}_{1\perp} \\ k_i &= \alpha_i p_2' + \beta_i p_1' + \boldsymbol{k}_{i\perp} \end{aligned}\right\}, \quad i = 1,2 \tag{8.3.3}$$

the denominators become

$$\left.\begin{aligned} d_1 &= \alpha_1\beta_1 s - \mu_1^2 + i\epsilon \\ d_2 &= (\alpha_1 - m^2/s)(\beta_1 - 1)s - \mu_2^2 + i\epsilon, \quad \text{etc.} \end{aligned}\right\} \tag{8.3.4}$$

where $$\mu_i^2 = m^2 + \boldsymbol{k}_{i\perp}^2$$

and the integration volumes become

$$d^4q_1 = \tfrac{1}{2}|s|\,d\alpha\,d\beta\,d^2\boldsymbol{q}_{1\perp} \quad \text{etc.} \tag{8.3.5}$$

Since $A^{R_1}(q_1,k_1,k_2)$ is a Regge pole amplitude we require that it should vanish if the momentum transfer becomes large, $q_1^2 \gg m^2$, and the 'masses' coupled to it, k_1^2, k_2^2, should also be $\gg m^2$. But its energy variable $s_1 = (k_1+k_2)^2 \approx 2k_1k_2 = \beta_1\alpha_2 s$ is large, so that the dominant region of integration in (8.3.1) is

$$\boldsymbol{q}_{1\perp}^2, \boldsymbol{k}_{1\perp}^2, \boldsymbol{k}_{2\perp}^2 \leqslant m^2; \quad \alpha,\beta,\alpha_1,\beta_2 \sim \frac{m^2}{s}; \quad \beta_1,\alpha_2 \sim 1$$

https://doi.org/10.1017/9781009403269.009 Published online by Cambridge University Press

Then with a factorized form for the Reggeon

$$A^{R_1}(q_1, k_1, k_2) = \gamma(q_1^2, k_1^2, (q_1 - k_1)^2) \times \gamma(q_1^2, k_2^2, (q_1 + k_2)^2)\, \xi_{\alpha_1(q_1^2)} (2k_1 k_2)^{\alpha_1(q_1^2)} \quad (8.3.6)$$

where $\alpha_1(q_1^2)$ is the Regge trajectory (not to be confused with the Sudakov variable α_1 in (8.3.3)!), and

$$\xi_{\alpha_1(q_1^2)} \equiv \frac{e^{-i\pi\alpha_1(q_1^2)} + \mathscr{S}_1}{\sin[\pi\alpha_1(q_1^2)]} \quad (8.3.7)$$

is the signature factor, and with a similar expression for A^{R_2}, we end up with

$$A^c(s,t) = \frac{ig^4}{2|s|} \int \frac{d^2\boldsymbol{q}_{1\perp}}{(2\pi)^2} N^2_{\alpha_1\alpha_2}(q, \boldsymbol{q}_{1\perp})\, s^{\alpha_1(q_1^2)\alpha_2(q_2^2)}\, \xi_{\alpha_1(q_1^2)}\, \xi_{\alpha_2(q_2^2)} \quad (8.3.8)$$

where

$$N_{\alpha_1\alpha_2} = \int \frac{d^2\boldsymbol{k}_{1\perp}}{(2\pi)^2} \frac{d\beta_1\, d\alpha_1\, d\alpha\, s^2 \gamma^2 (\beta_1)^{\alpha_1(q_1^2)} (1-\beta_1)^{\alpha_2(q_2^2)}}{\prod_{m=1}^{4} d_m} \quad (8.3.9)$$

is the Feynman integral over the upper cross, and is the same as (8.2.36) except for the incorporation of γ^2, and the occurrence of the Sudakov parameters raised to the power $\alpha(q^2)$, due to the spins of the Reggeons.

The result (8.3.8) obviously agrees with (8.2.37) except that we have now included the signature factors of the Reggeons properly (remembering (8.2.13)). The two-dimensional nature of the remaining integration agrees with the results (3.4.9) and (8.2.13), and stems from the fact that after partial-wave projection (over two angles) only two of the four space–time dimensions remain to be integrated over. It is evident that the signature of this cut is just the product of the signatures of the two poles, i.e.

$$\mathscr{S}_c = \mathscr{S}_1 \mathscr{S}_2 \quad (8.3.10)$$

This is because $|s|$ appears in the denominator, so that under $s \to -s$ A^c transforms like the product of the poles. The four terms obtained from multiplying the two signature factors are shown in fig. 8.11.

To examine the J-plane structure we take the Mellin transform (2.10.3),

$$A_J(t) = \frac{1}{\pi} \int_0^\infty D_s(s,t)\, s^{-J-1}\, ds \quad (8.3.11)$$

https://doi.org/10.1017/9781009403269.009 Published online by Cambridge University Press

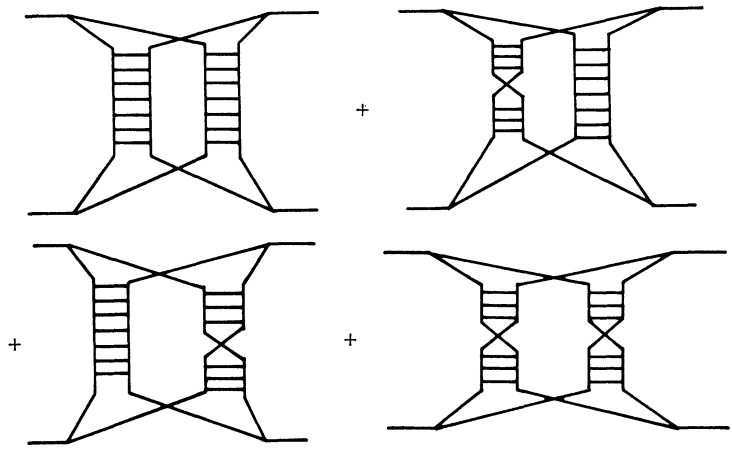

FIG. 8.11 The set of four diagrams, including crossed terms $s \leftrightarrow u$, obtained from the product of the signature factors in (8.3.8).

with the s-discontinuity of (8.3.8),

$$D_s = \frac{g^4}{2|s|}\int \frac{\mathrm{d}^2\boldsymbol{q}_{1\perp}}{(2\pi)^2} N^2_{\alpha_1\alpha_2}(q, \boldsymbol{q}_{1\perp})\, s^{\alpha_1(q_1^2)+\alpha_2(q_2^2)} \operatorname{Re}\{\xi_{\alpha_1}\xi_{\alpha_2}\} \tag{8.3.12}$$

where from (8.3.7)

$$\operatorname{Re}\{\xi_{\alpha_1}\xi_{\alpha_2}\} = \cos\left[\frac{\pi}{2}\left(\alpha_1+\alpha_2+\sum_{i=1,2}\frac{1-\mathscr{S}_i}{2}\right)\right] \tag{8.3.13}$$

and obtain $$A_J(t) = \frac{g^4}{2}\int \frac{\mathrm{d}^2\boldsymbol{q}_{1\perp}}{(2\pi)^2} \frac{N^2_{\alpha_1\alpha_2}(q, \boldsymbol{q}_{1\perp}) \operatorname{Re}\{\xi_{\alpha_1}\xi_{\alpha_2}\}}{J+1-\alpha_1(q_1^2)-\alpha_2(q_2^2)} \tag{8.3.14}$$

which exhibits the cut at

$$\begin{aligned} J &= \max\{\alpha_1(q_1^2)+\alpha_2((q-q_1)^2)-1\} \\ &= \max\{\alpha_1(-\boldsymbol{q}_{1\perp}^2)+\alpha_2(-(\boldsymbol{q}_\perp-\boldsymbol{q}_{1\perp})^2)-1\} \end{aligned} \tag{8.3.15}$$

corresponding to (8.2.19).

The discontinuity across this two-Reggeon cut is

$$\begin{aligned} \Delta_2(J,t) \equiv \Delta_{J_2}\{A_J(t)\} = \mathrm{i}g^4 \int \frac{\mathrm{d}^2\boldsymbol{q}_{1\perp}}{(2\pi)^2} N^2_{\alpha_1\alpha_2}(q, \boldsymbol{q}_{1\perp}) \\ \times \operatorname{Re}\{\xi_{\alpha_1}\xi_{\alpha_2}\}\, \delta(J+1-\alpha_1(q_1^2)-\alpha_2(q_2^2)) \end{aligned} \tag{8.3.16}$$

which may be rewritten

$$\begin{aligned} \Delta_{J_2}\{A_J(t)\} = (-1)\sin\left[\frac{\pi}{2}\left(J-\sum_i\frac{1-\mathscr{S}_i}{2}\right)\right]\mathrm{i}g^4 \\ \times \int \frac{\mathrm{d}^2\boldsymbol{q}_{1\perp}}{(2\pi)^2}\int \frac{\mathrm{d}^2\boldsymbol{q}_{2\perp}}{(2\pi)^2}(2\pi)^2\delta^2(\boldsymbol{q}_{1\perp}+\boldsymbol{q}_{2\perp}-\boldsymbol{q}_\perp) \\ \times \delta(J+1-\alpha_1(-\boldsymbol{q}_{1\perp}^2)-\alpha_2(-\boldsymbol{q}_{2\perp}^2))\, N^2_{\alpha_1\alpha_2} \end{aligned} \tag{8.3.17}$$

https://doi.org/10.1017/9781009403269.009 Published online by Cambridge University Press

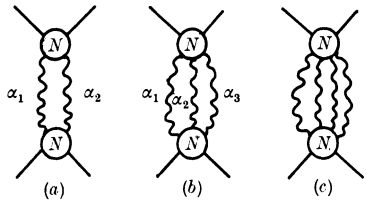

FIG. 8.12 Some multi-Reggeon cuts.

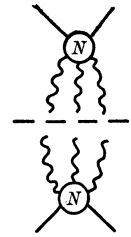

FIG. 8.13 Discontinuity across the three-Reggeon cut. Each Reggeon has momentum $\boldsymbol{q}_{i\perp}$ and 'energy' $E_i = 1-\alpha_i(-\boldsymbol{q}_{i\perp}^2)$.

Similarly for higher order cuts such as fig. 8.12 the discontinuity is

$$\Delta_{J_n}\{A_J(t)\} = (-1)^{n-1}\sin\left[\frac{\pi}{2}\left(J-\sum_i\frac{1-\mathscr{S}_i}{2}\right)\right] ig^{2n} \times \int\frac{\mathrm{d}^2\boldsymbol{q}_{1\perp}}{(2\pi)^2}\ldots\int\frac{\mathrm{d}^2\boldsymbol{q}_{n\perp}}{(2\pi)^2}(2\pi)^2\delta^2(\boldsymbol{q}_{1\perp}+\ldots+\boldsymbol{q}_{n\perp}-\boldsymbol{q}_\perp) \times\delta(J+n-1-\sum_i\alpha_i(-\boldsymbol{q}_{1\perp}^2))\,N^2_{\alpha_1\ldots\alpha_n} \quad (8.3.18)$$

This equation can be regarded as the discontinuity across the Feynman graph like fig. 8.13, in which each Reggeon is regarded as a quasi-particle in a two-dimensional space, with momentum $\boldsymbol{q}_{i\perp}$ and 'energy' $E_i = 1-\alpha_i(-\boldsymbol{q}_{1\perp}^2)$, the 'energy' and momentum being conserved at each vertex, since the δ-functions in (8.3.18) then correspond to those of the Cutkosky rules (1.5.11). The 'phase space' is

$$\prod_i\frac{\mathrm{d}^2\boldsymbol{q}_{i\perp}}{(2\pi)^2}(2\pi)^2\delta(\sum_i\boldsymbol{q}_{i\perp}-\boldsymbol{q}_\perp)\,2\pi\delta(\sum_i E_i-E)\equiv\mathrm{d}\Phi_n^J \quad (8.3.19)$$

where $E\equiv 1-J$, and (8.3.18) can be rewritten as

$$\Delta_{J_n}\{A_J(t)\} = (-1)^{n-1}\sin\left[\frac{\pi}{2}\left(1-E-\sum_i\frac{1-\mathscr{S}_i}{2}\right)\right] ig^{2n}\int\mathrm{d}\Phi_n^J\,N^2_{E_1\ldots E_n} \quad (8.3.20)$$

The next step is to try and generalize the above prescription so that the N's instead of being just Feynman integrals, can themselves contain Reggeon amplitudes. Thus N may be expected to contain Regge poles and cuts like fig. 8.14. This is more complicated, however, because it is necessary to be clear about which side of their branch cuts the N's in the above formulae are to be evaluated. To determine this it is necessary to regard the Reggeons as two-body states (at

https://doi.org/10.1017/9781009403269.009 Published online by Cambridge University Press

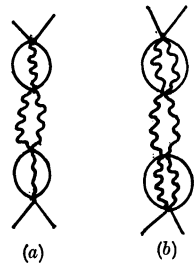

FIG. 8.14 (*a*) Pole and (*b*) cut contributions to the N's in fig. 8.12(*a*).

least), and so the two-Reggeon cut involves four-body unitarity in the t channel.

It turns out (Gribov, Pomeranchuk and Ter-Martirosyan 1965, White 1972, 1974) that the results are almost exactly analogous to the discontinuity formulae for s-plane singularities, and we can write, for example (cf. (1.3.16)),

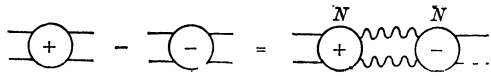

(8.3.21)

or

$$\Delta_{J_2}\{A_J(t)\} = (-1)\sin\left[\frac{\pi}{2}\left(J - \sum_i \frac{1-\mathscr{S}_i}{2}\right)\right]\int \mathrm{d}\Phi_2^J N_{\alpha_1\alpha_2}(J_+)\, N_{\alpha_1\alpha_2}(J_-) \tag{8.3.22}$$

where $J_\pm \equiv J \pm \mathrm{i}\epsilon$ are evaluated above/below the cuts in N. This generalization looks rather obvious, but in fact a great deal of care is needed to ensure that the correct discontinuities have been taken, particularly keeping in mind the signature properties of the Reggeons.

This similarity between the unitarity equations in the s plane and the J plane, with the Cutkosky-like rule (8.3.22) has led various authors to try and construct a Reggeon field theory in a space with two spacelike and one timelike dimension (Gribov and Migdal 1968, 1969, Cardy and White 1973, 1974, Migdal, Polyakov and Ter-Martirosyan 1974, Abarbanel and Bronzan 1974*a*, *b*). For linear trajectories

$$\alpha(-\boldsymbol{K}^2) = \alpha^0 - \alpha'\boldsymbol{K}^2$$

the Regge pole becomes

$$\frac{1}{J-\alpha} \to \frac{1}{E - \alpha'\boldsymbol{K}^2 + (1-\alpha^0)} \tag{8.3.23}$$

reminiscent of the propagator of a non-relativistic particle of mass $m = (2\alpha')^{-1}$ (cf. (1.13.25)), and with an 'energy gap' $1-\alpha_0$, i.e. the

velocity is $v = [4\alpha'(E-1+\alpha^0)]^{\frac{1}{2}}$. So one can produce a field theory in which the Reggeon field obeys the Schroedinger equation. There are the usual problems of re-normalization (see fig. 8.14) and convergence, compounded by a fundamental uncertainty as to whether it makes sense to replace ladders by bare Reggeons and then re-normalize them. For example the presence of a pole or cut above $J = -1$ in N means that $A(s_1, t, t_1, t_2)$ in (8.2.38) $\sim s_1^{\alpha(t)}$ or $\sim s_1^{\alpha_c(t)}$, and so the integral defining N will not converge without re-normalization. What is worse, for the P with $\alpha^0 = 1$ there is no energy gap, so the P is analogous to a massless particle in conventional field theory, and all the singularities pile up at $J = 1$, just like the 'infra-red' problem caused by the massless photon in quantum electrodynamics. The asymptotic behaviour of cross-sections thus depends on the solutions near the critical point $J = 1$. These have been studied using re-normalization group methods. So far only limited progress has been made with this approach, and we shall not pursue it further (see Abarbanel *et al.* (1975) for a review).

To summarize and generalize these results, we have found that the exchange of n Reggeons $R_1, \ldots, R_n$ gives rise to a cut branch point at (from (8.3.18), cf. (8.2.19))

$$\alpha_{c_n}(t) = \max\left\{\sum_{i=1}^{n} \alpha_i(t_i) - n + 1\right\} \tag{8.3.24}$$

where the maximum value is over the allowed region of integration, and for increasing trajectories this is bounded by (cf. (8.2.18))

$$\sum_{i=1}^{n} \sqrt{-t_i} = \sqrt{-t} \tag{8.3.25}$$

We shall often refer to this as the $\mathrm{R}_1 \otimes \mathrm{R}_2 \otimes \ldots \otimes \mathrm{R}_n$ Regge cut, where the $\otimes$ implies the phase-space integration (8.3.8) or (8.3.18). If the trajectories are identical these rules give

$$\alpha_{c_n}(t) = n\alpha(t/n^2) - n + 1 \tag{8.3.26}$$

and if they are linear, $\alpha(t) = \alpha^0 + \alpha' t$,

$$\alpha_{c_n}(t) = \alpha' t/n + n(\alpha^0 - 1) + 1 \tag{8.3.27}$$

The signature of the cut is the product of the signatures of the poles (cf. (8.3.10))

$$\mathscr{S}_c = \prod_i \mathscr{S}_i \tag{8.3.28}$$

We remarked in the introduction that Regge cuts are necessary to

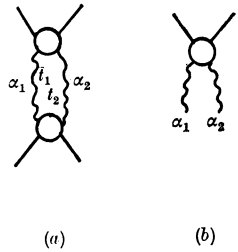

FIG. 8.15 (*a*) Two-Reggeon intermediate state in the t channel. (*b*) Reggeon–particle scattering amplitude.

ensure consistency of the Gribov–Pomeranchuk fixed poles with t-channel unitarity, and we should check that the above branch points can do this (see Jones and Teplitz 1967, Bronzan and Jones 1967, Schwarz 1967, Hwa 1967).

For scalar external particles the highest Gribov–Pomeranchuk singularity is at $J = -1 \equiv J_0$, say, in an even-signature amplitude. If the Regge cut is to overlie the t-channel unitarity cut beginning at the threshold $t = t_T = 4m^2$, we obviously require that $\alpha_c(t_T) = J_0$. If the particles constituting this threshold (fig. 8.15) lie on trajectories $\alpha(t)$, we must have $\alpha(m^2) = 0$ for scalar particles, and substituting this in (8.3.26) for $n = 2$ we get

$$\alpha_{c_2}(4m^2) = 2\alpha(m^2) - 1 = -1 \tag{8.3.29}$$

so the cut branch point coincides with the fixed pole at threshold. Then if we continue in t_1 and t_2 up the trajectories to α_1, α_2 = integers > 0, the highest Gribov–Pomeranchuk pole in the amplitude fig. 8.15 (*a*) will be at $J = \alpha_1 + \alpha_2 - 1$, since α_1 is the largest possible helicity for a particle of spin α_1, and the Reggeon branch point evidently remains in the correct place to prevent conflict with unitarity. The full cut structure is a good deal more complicated than this brief account suggests, however, particularly for unequal mass particles – see Schwarz (1967) and Olive and Polkinghorne (1968).

In the t plane the branch point occurs at $t = t_c(J)$ where $t_c(J)$ is defined by

$$\alpha_c(t_c(J)) = J \tag{8.3.30}$$

So, from (8.3.29), $t_c(-1) = 4m^2$. As J is increased from -1, t_c moves along the elastic branch cut until the first inelastic threshold t_I is reached, whereupon it passes through the inelastic branch cut on to the unphysical sheet. So $\alpha_c(t)$ has a branch point at J_I where $t_c(J_I) = t_I$, and the cut discontinuity $\Delta_2(J, t)$ has a branch point here.

This connection between the Gribov–Pomeranchuk poles and the cuts is of course not accidental but arises because the cuts are generated by the fixed poles in the cross diagram N (fig. 8.6(*e*)) through two-Reggeon unitarity. The way in which this works in perturbation theory was demonstrated by Olive and Polkinghorne (1968), and Landshoff and Polkinghorne (1969). If we write the cross as

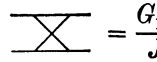

$$= \frac{G_1(t,J)}{J+1}$$

then the next-order diagram is

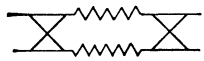

$$= \frac{G_2(t,J)}{J+1}$$

and the discontinuity of G_2 across the cut must contain the fixed pole, so

$$\mathrm{Disc}_2\{G_2\} = \frac{\rho G_1}{J+1}$$

where ρ is a phase-space factor. So from these two diagrams we have, above the cut,

$$A_J^{\mathrm{I}} = \frac{G_1+G_2}{J+1} \tag{8.3.31}$$

but below the cut, $$A_J^{\mathrm{II}} = \frac{G_1+G_2}{J+1} + \frac{\mathrm{i}\rho G_1^2}{(J+1)^2} \tag{8.3.32}$$

This appears to have generated a double pole, but using the t-channel unitarity equation (i.e. like (2.2.7) with $A_J^{\mathrm{I}} \equiv A_J(t_+)$, $A_J^{\mathrm{II}} = A(t_-)$) we get

$$A_J^{\mathrm{II}} = \frac{A_J^{\mathrm{I}}}{1-\mathrm{i}\rho A_J^{\mathrm{I}}} = A_J^{\mathrm{I}} + \mathrm{i}\rho(A_J^{\mathrm{I}})^2 + (\mathrm{i}\rho)^2(A_J^{\mathrm{I}})^3 + \ldots \tag{8.3.33}$$

so if to all orders

$$A_J^{\mathrm{I}} = \frac{G}{J+1}, \quad G = G_1 + G_2 + \ldots \tag{8.3.34}$$

then $$A_J^{\mathrm{II}} = \frac{G}{J+1-\mathrm{i}\rho G} = \frac{G}{J+1} + \frac{\mathrm{i}\rho G^2}{(J+1)^2} + \ldots \tag{8.3.35}$$

i.e. A_J^{II} contains a sequence of multiple poles which sum to give a finite value for A_J^{II} as $J \to -1$. So the cut sequence, fig. 8.16, permits there to be a fixed pole on the physical sheet (I) and nothing worse. Such cuts are clearly essential if continuation in angular momentum is to be compatible with t-channel unitarity in any theory which includes a third double spectral function ρ_{su}.

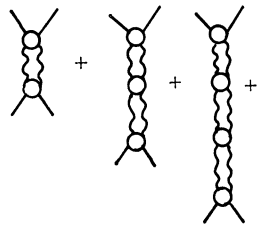

FIG. 8.16 The t-channel iteration of two-Reggeon cut.

However, if the presence of this cut discontinuity is to be compatible with the t-channel elastic unitarity condition (8.3.33) we need (Bronzan and Jones 1967), for $t > t_T$,

$$\Delta_t\{A_J(t)\} \to 0 \quad \text{as} \quad t \to t_c(J) \tag{8.3.36}$$

and so

$$\Delta_J\{A_J(t)\} \to 0 \quad \text{as} \quad J \to \alpha_c(t) \tag{8.3.37}$$

i.e. the discontinuity across the Regge cut must vanish at the branch point. This is not true of the cut (8.3.8) which, as we have seen in (8.2.16), gives

$$A(s,t) \sim s^{\alpha_c}(\log s)^{-1} \quad \text{and so} \quad A_J(t) \sim \log(J-\alpha_c) \tag{8.3.38}$$

(from (2.7.4)). And of course the logarithm has a finite discontinuity ($= \pi$) between one sheet and the next at $J = \alpha_c$. However, t-channel unitarity requires that we include the full sequence of cuts, fig. 8.16, and so $N_{\alpha_1\alpha_2}$ in (8.3.8) will contain the two-Reggeon cut (fig. 8.14(*b*)) and so satisfies the unitarity condition (White 1972)

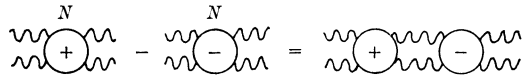

or

$$N(J_+) - N(J_-) \underset{J\to\alpha_c}{\sim} i\pi N(J_+)\,N(J_-) \tag{8.3.39}$$

so

$$\frac{1}{N(J_+)} - \frac{1}{N(J_-)} \underset{J\to\alpha_c}{\sim} -i\pi$$

i.e.

$$\frac{1}{N(J)} \sim \log(J-\alpha_c)$$

which in (8.3.16) gives

$$\Delta\{A_J(t)\} \underset{J\to\alpha_c}{\sim} (\log(J-\alpha_c))^{-2} \tag{8.3.40}$$

so the singularity is softened to an inverse logarithmic cut, not a logarithm.

https://doi.org/10.1017/9781009403269.009 Published online by Cambridge University Press

Substituted in (2.7.8) this gives

$$A^{c}(s,t) \underset{s\to\infty}{\sim} \int^{\alpha_c} \mathrm{d}J \frac{1}{(\log(J-\alpha_c))^2} s^J \sim s^{\alpha_c} \int^0 \mathrm{d}x \frac{\mathrm{e}^{x\log s}}{(\log x)^2}$$

$$\sim \frac{s^{\alpha_c}}{\log s} \int^1 \frac{\mathrm{d}y}{(\log(\log y) - \log(\log s))^2} \sim \frac{s^{\alpha_c}}{\log s (\log(\log s))^2} \quad (8.3.41)$$

(where we have made the successive substitutions $x = J - \alpha_c$, $\log y = x \log s$). Since $\log(\log s)$ varies so slowly with s, this correction is of very little practical importance, but it is necessary to keep in mind that compatibility with t-channel unitarity involves not just fig. 8.15, but the infinite sum fig. 8.16. Unitarization makes even less difference to three-and-more-Reggeon cuts since (8.3.20) gives $A^{c}_{J}(t) \sim (J-\alpha_c)^{n-2} \log(J-\alpha_c)$ which for $n > 2$ already has a vanishing discontinuity at the branch point, and through (2.7.4) produces the asymptotic behaviour $\sim s^{\alpha_c} (\log s)^{-(n-1)}$.

8.4 The absorption and eikonal models

Although the Feynman-diagram models and the Reggeon calculus have told us a good deal about the properties to be expected of Regge cuts, they do not give the strength of the cuts relative to the poles, and so give very little idea of how important cuts are likely to be in practice.

Thus (8.2.37) and (8.3.8) suggest that for a two-Reggeon cut amplitude, $\mathrm{R}_1 \otimes \mathrm{R}_2$, we should write

$$A^{c}(s,t) = \frac{\mathrm{i}}{16\pi^2 |s|} \iint_{-\infty}^{0} \mathrm{d}t_1 \, \mathrm{d}t_2 \frac{\theta(-\lambda)}{(-\lambda(t,t_1,t_2))^{\frac{1}{2}}}$$

$$\times (N(t,t_1,t_2))^2 A^{\mathrm{R}_1}(s,t_1) A^{\mathrm{R}_2}(s,t_2) \quad (8.4.1)$$

where the A^{R_i} are physical Regge pole amplitudes. We have absorbed g^2 into the definition of the vertices N which should include all contributions to ρ_{su}, and is of course unknown (but see section 10.9). However, various models have been suggested for calculating cuts which reproduce a structure like (8.4.1) but with a specific prescription for N, and we review two of them here. Though neither is particularly compelling both do at least have the merit of providing a simple way of including spin-kinematics etc.

https://doi.org/10.1017/9781009403269.009 Published online by Cambridge University Press

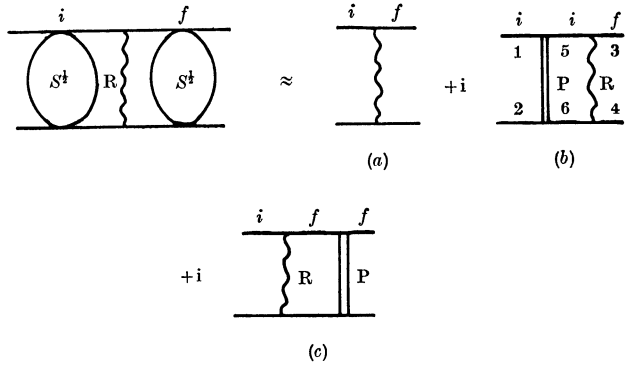

FIG. 8.17 Reggeized absorption model.

a. The Reggeized absorption model

This is used for inelastic reactions where quantum numbers are exchanged. The basic idea is to use a Regge pole, R, to carry the exchanged quantum numbers, but to include modifications caused by elastic scattering in the initial and final states, as in fig. 8.17. Since the elastic amplitude is predominantly imaginary the effect is to reduce the lower partial waves, which corresponds physically to absorption of the incoming flux into channels other than those being considered. It is possible to use the full elastic scattering amplitude, but it is more illuminating to represent it by its dominant Regge pole, the Pomeron, P.

Specifically the hypothesis is that the s-channel partial waves for the processes $1+2$ (channel i) $\to 3+4$ (channel f) may be written in the form (Henyey *et al.* 1969)

$$A_J^{if}(s) = (S_J^{ii}(s))^{\frac{1}{2}} A_J^{if}(s) (S_J^{ff}(s))^{\frac{1}{2}} \tag{8.4.2}$$

where $A_J^{if\mathrm{R}}(s)$ is the s-channel partial-wave projection of the t-channel Reggeon, and $S_J^{ii}(s)$ is the partial-wave S-matrix for elastic scattering in the initial state, etc. Since we shall want to sum over all the helicities of the particles it is convenient to regard i and f as helicity labels, and (8.4.2) as a matrix product relation. Then we write the elastic S-matrix as

$$S_J^{ii}(s) \approx 1 + 2i\rho(s) A_J^{ii\mathrm{P}}(s) \tag{8.4.3}$$

where $A_J^{ii\mathrm{P}}(s)$ is the partial-wave projection of the P exchange amplitude and $\rho^i(s) = 2q_{s12}s^{-\frac{1}{2}}$ is the kinematical factor (2.2.9). On substituting (8.4.3), and a similar expression for S_J^{ff}, into (8.4.2), and

https://doi.org/10.1017/9781009403269.009 Published online by Cambridge University Press

expanding the square-roots, we get

$$A^{if}_J(s) \approx A^{if\,\mathrm{R}}_J(s) + \mathrm{i}\rho^i(s)\, A^{ii\,\mathrm{P}}_J(s)\, A^{if\,\mathrm{R}}_J(s) + \mathrm{i}\rho^f(s)\, A^{if\,\mathrm{R}}_J(s)\, A^{ff\,\mathrm{P}}_J(s) + \ldots \quad (8.4.4)$$

The first term is just the Reggeon R, while the second and third terms give cuts due to the exchange of R and P together, i.e. $\mathrm{R}\otimes\mathrm{P}$ cuts. The full amplitude is obtained by summing the partial-wave series (4.4.9). So for example from the second term in (8.4.4) we get

$$A^{\mathrm{R}\otimes\mathrm{P}}_{H_s}(s,t) = \mathrm{i}\rho^i(s)\, 16\pi \sum_J (2J+1) \sum_{\mu_5\mu_6} A^{ii\,\mathrm{P}}_{\mu_1\mu_2\mu_5\mu_6 J}(s)\, A^{if\,\mathrm{R}}_{\mu_5\mu_6\mu_3\mu_4 J}(s)\, d^J_{\mu\mu'}(z_s)$$
$$\mu = \mu_1 - \mu_2, \quad \mu' = \mu_3 - \mu_4 \quad (8.4.5)$$

Then if we make a partial-wave projection of the pole amplitudes (dropping the channel labels for simplicity), we get

$$A^{\mathrm{R}\otimes\mathrm{P}}_{H_s}(s,t) = \sum_{\mu_5\mu_6} \mathrm{i}\rho(s)\, 16\pi \sum_J (2J+1)\, d^J_{\mu\mu'}(z_s) \frac{1}{32\pi} \int_{-1}^{1} A^{\mathrm{P}}_{\mu_1\mu_2\mu_5\mu_6}(s,z_1) \times d^J_{\mu\mu''}(z_1)\, \mathrm{d}z_1 \frac{1}{32\pi} \int_{-1}^{1} A^{\mathrm{R}}_{\mu_5\mu_6\mu_3\mu_4}(s,z_2)\, d^J_{\mu''\mu'}(z_2)\, \mathrm{d}z_2, \quad \mu'' = \mu_5 - \mu_6 \quad (8.4.6)$$

where z_1 and z_2 are the cosines of the scattering angles between the initial and intermediate, and intermediate and final states, respectively (see fig. 2.1), which satisfy (2.2.4), viz.

$$z_1 = zz_2 + (1-z^2)^{\frac{1}{2}}(1-z_2^2)^{\frac{1}{2}} \cos\phi \quad (8.4.7)$$

But (Henyey *et al.* 1969)

$$\sum_J (2J+1)\, d^J_{\mu\mu'}(z_s)\, d^J_{\mu\mu''}(z_1)\, d^J_{\mu''\mu'}(z_2) = \frac{2}{\pi} \frac{\theta(\Delta)}{\Delta^{\frac{1}{2}}} \cos(\mu\phi_1 + \mu'\phi_2 + \mu''\phi_3) \quad (8.4.8)$$

(cf. (8.2.6)) and in the high-energy limit (8.2.10) the ϕ dependence may be neglected, and $\rho(s)\to 1$, and so we obtain

$$A^{\mathrm{R}\otimes\mathrm{P}}_{H_s}(s,t) = \sum_{\mu_5\mu_6} \frac{\mathrm{i}}{16\pi^2|s|} \iint_{-\infty}^{0} \mathrm{d}t_1\, \mathrm{d}t_2\, A^{\mathrm{P}}_{\mu_1\mu_2\mu_5\mu_6}(s,t_1)\, A^{\mathrm{R}}_{\mu_5\mu_6\mu_3\mu_4}(s,t_2) \times \frac{\theta(-\lambda)}{(-\lambda(t,t_1,t_2))^{\frac{1}{2}}} \quad (8.4.9)$$

which is identical with (8.4.1) for spinless scattering, with $N(t,t_1,t_2) = 1$. It also agrees with the AFS result (8.2.11) except for the complex conjugation of the Reggeon amplitude. In fact (8.2.11) corresponds to taking

$$\mathrm{Im}\{\mathrm{A}^{\mathrm{c}}_J(s)\} = \rho^i(s)\, \mathrm{Re}\{A^{ii\,\mathrm{P}}_J(s)\, (A^{if\,\mathrm{R}}_J(s))^*\} \quad (8.4.10)$$

https://doi.org/10.1017/9781009403269.009 Published online by Cambridge University Press

instead of (8.4.4). However, since the P is almost pure imaginary this complex conjugation would give essentially the opposite sign for the cut. The absorptive sign in (8.4.9) agrees with the Mandelstam result (8.2.37), and the Reggeon calculus (8.3.8), rather than the AFS sign of (8.2.11).

There are some fairly obvious defects in this approach. First, fig. 8.17(*b*) is a planar diagram, and we found in section 8.2 that planar diagrams should not give rise to cuts. The reason why we get a similar answer is that the particle propagators across the diagram $\sim 1/s$, and so have the same power behaviour as the crosses of fig. 8.6, but really fig. 8.17(*b*) looks more like a re-normalization of the box-diagram contribution to the Regge pole in fig. 8.1. Secondly, if the Reggeon is regarded as a ladder it already includes inelastic intermediate states in the s channel, and so to absorb it again may involve double counting. This is clearly related to the re-normalization problem. However, we shall find in section 8.6 that one of the main defects of Regge poles is that they give too large a contribution to the low partial waves, so phenomenologically some extra absorption is certainly necessary, and probably should be provided by cuts. Also the elastic intermediate state $|5,6\rangle$ is only one of a large number of diffractively produced states which can arise through P exchange, and we should probably consider the sum of all diagrams like fig. 8.18. They are sometimes included rather crudely by multiplying (8.4.9) by an enhancement factor $\lambda > 1$. Note that λ must be independent of s, otherwise the position of the cut will be moved, despite the fact that more diffractive states open as s is increased.

We thus conclude that though the absorption idea is useful in confirming the basic form of (8.4.1), it cannot be taken too seriously as a quantitative model for Regge cuts.

b. The eikonal model

This is directly related to the eikonal method for high energy potential scattering discussed in section 1.14, and it gives a way of computing the high energy limit of sums of diagrams like fig. 8.29 corresponding to many-Reggeon exchange (Arnold 1967). In fact, however, the nature of the exchange is not very important so we begin by considering the exchange of scalar particles rather than Reggeons (see Levy and Sucher 1969, Abarbanel and Itzykson 1969, Chang and Yan 1970, Tiktopoulos and Trieman 1971, Cardy 1971).

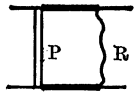

FIG. 8.18 Diffractively produced intermediate states in the absorption model giving additional terms in (8.8.4).

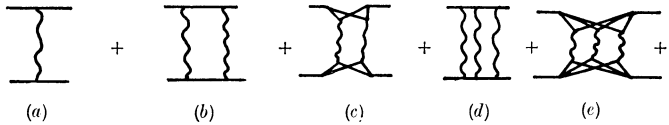

FIG. 8.19 A sequence of multi-Reggeon exchange diagrams.

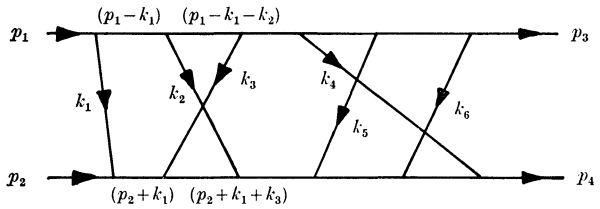

FIG. 8.20 A crossed-rung ladder.

A typical n-rung diagram is fig. 8.20, a generalized ladder in which some of the rungs cross over each other. The Feynman rules give

$$A^n(s,t) = g^{2n} \prod_{i=1}^{n} \int \frac{\mathrm{d}^4 k_i}{(2\pi^4)} \frac{1}{k_i^2 - m^2} (2\pi)^4 \delta^4(p_1 - p_1' - \Sigma k_i)$$
$$\times \{[(p_1-k_1)^2-m^2][(p_1-k_1-k_2)^2-m^2]\ldots[(p_1-k_1-\ldots-k_n)^2-m^2]$$
$$\times [(p_2+k_1)^2-m^2]\ldots[(p_2+k_1+\ldots+k_n)^2-m^2]\}^{-1} \qquad (8.4.11)$$

We work in the high energy small-angle scattering approximation in which very little momentum is given up to each of the rungs, so the recoil of particles 1 and 2 at each successive scattering is small, in which case we can make the replacement

$$(p_1 \pm k)^2 - m^2 = \pm 2p_1.k + k^2 \approx \pm 2p_1.k \qquad (8.4.12)$$

throughout. This clearly corresponds to the eikonal assumptions of section 1.14. It is then necessary to sum over all permutations of the ordering of the rungs arriving at particle 2 for the given ordering $k_1 \ldots k_n$ of rungs leaving particle 1. With the approximations (8.4.12) the symmetry of the integrand makes it possible with some effort (see Levy and Sucher (1969) for details) to rearrange the sum over

https://doi.org/10.1017/9781009403269.009 Published online by Cambridge University Press

permutations to a remarkably simple form. The integrations can then be performed by transforming into x space using

$$\frac{1}{k_i^2-m^2} = \int \mathrm{d}^4x \Delta_{\mathrm{F}}(x)\, \mathrm{e}^{-\mathrm{i}k_i\cdot x} \tag{8.4.13}$$

where the Feynman propagator is

$$\Delta_{\mathrm{F}}(x) = \frac{\mathrm{i}}{(2\pi)^4}\int \mathrm{d}^4k \frac{\mathrm{e}^{\mathrm{i}k\cdot x}}{k^2-m^2+\mathrm{i}\epsilon} \tag{8.4.14}$$

and on summation it is found that

$$A^n(s,t) = \frac{g^2}{n!}\int \mathrm{d}^4x\, \mathrm{e}^{-\mathrm{i}q\cdot x}\Delta_{\mathrm{F}}(x)\,(\mathrm{i}\chi)^{n-1} \tag{8.4.15}$$

where $$q \equiv p_1 - p_3$$

and

$$\chi \equiv -(U(x,p_1,p_2)+U(x,p_1,-p_4)+U(x,-p_3,p_2)+U(x,-p_2,-p_4)) \tag{8.4.16}$$

where

$$U(x,p_i,p_j) \equiv g^2\int \frac{\mathrm{d}^4k}{(2\pi)^4}\frac{\mathrm{e}^{\mathrm{i}k\cdot x}}{(k^2-m^2+\mathrm{i}\epsilon)(-2p_i.k+\mathrm{i}\epsilon)(2p_j.k+\mathrm{i}\epsilon)} \tag{8.4.17}$$

Clearly in the high energy, small-angle limit $p_3 \simeq p_1$, $p_2 \simeq p_4$ so χ depends only on $2p_1.p_2$ (i.e. s), $p_1.k$ and $p_2.k$. On performing the contour integration in k contributions appear just from the vanishing of the denominators, so putting $(2p_i.k+\mathrm{i}\epsilon)^{-1}\to 2\pi\mathrm{i}\delta(2p_i.k)$ the four terms in (8.4.16) give

$$\chi(x,p_1,p_2) = \frac{g^2}{(2\pi)^2}\int \mathrm{d}^4k \frac{\mathrm{e}^{\mathrm{i}k\cdot x}}{k^2-m^2+\mathrm{i}\epsilon}\,\delta(2p_1.k)\,\delta(2p_2.k) \tag{8.4.18}$$

and integrating k in the plane of p_1 and p_2 (see fig. 1.12) this becomes

$$\chi(s,\mathbf{b}) = \frac{g^2}{8\pi^2 s}\int \mathrm{d}^2\boldsymbol{k}\frac{\mathrm{e}^{-\mathrm{i}\mathbf{k}\cdot\mathbf{b}}}{t-m^2+\mathrm{i}\epsilon} \tag{8.4.19}$$

We can then perform the ϕ integration as in (1.14.10) to obtain

$$\chi(s,b) = \frac{1}{8\pi s}\int_{-\infty}^{0} \mathrm{d}t\, J_0(b\sqrt{-t})\frac{g^2}{t-m^2} \tag{8.4.20}$$

of which the inverse is (from (1.14.14))

$$\frac{g^2}{t-m^2} = 4\pi s\int_0^\infty b\,\mathrm{d}b\, J_0(b\sqrt{-t})\,\chi(s,b) = A^{\mathrm{B}}(s,t) \tag{8.4.21}$$

https://doi.org/10.1017/9781009403269.009 Published online by Cambridge University Press

which from (8.4.13) $$= g^2 \int \mathrm{d}^4x \, \Delta_{\mathrm{F}}(x) \, \mathrm{e}^{-\mathrm{i}q \cdot x} \tag{8.4.22}$$

in the high energy, small-angle approximation. So (8.4.15) gives

$$A^n(s,t) = \frac{4\pi s}{n!} \int_0^\infty b \, \mathrm{d}b \, J_0(b\sqrt{-t}) \, \chi(s,b) \, (\mathrm{i}\chi(s,b))^{n-1} \tag{8.4.23}$$

and on summing over all possible numbers of rungs we get

$$A(s,t) = \sum_{n=1}^{\infty} A^n(s,t) = 8\pi s \int_0^\infty b \, \mathrm{d}b \, J_0(b\sqrt{-t}) \frac{\mathrm{e}^{\mathrm{i}\chi(s,b)} - 1}{2\mathrm{i}} \tag{8.4.24}$$

The first term of this series ($n = 1$) is just (8.4.21), the single-particle-exchange Born approximation. The second term is the sum of all the two-particle exchange graphs

$$A^2(s,t) = 4\pi s \int_0^\infty b \, \mathrm{d}b \, J_0(b\sqrt{-t}) \frac{\mathrm{i}\chi^2}{2} \tag{8.4.25}$$

which when we substitute (8.4.20) gives

$$A^2(s,t) = 2\pi s \mathrm{i} \int_0^\infty b \, \mathrm{d}b \, J_0(b\sqrt{-t}) \frac{1}{(8\pi s)^2} \times \int_{-\infty}^0 \mathrm{d}t_1 J_0(b\sqrt{-t_1}) \, A^{\mathrm{B}}(s,t_1) \int_{-\infty}^0 \mathrm{d}t_2 J_0(b\sqrt{-t_2}) \, A^{\mathrm{B}}(s,t_2) \tag{8.4.26}$$

But (Heneyey *et al.* 1969, Erdelyi *et al.* (1953) vol. 2)

$$\int_0^\infty b \, \mathrm{d}b \, J_0(b\sqrt{-t_1}) \, J_0(b\sqrt{-t_2}) \, J_0(b\sqrt{-t}) = \frac{2}{\pi} \frac{\theta(-\lambda)}{(-\lambda(t,t_1,t_2))^{\frac{1}{2}}} \tag{8.4.27}$$

(cf. (8.2.6) and (8.4.8)) so

$$A^2(s,t) = \frac{\mathrm{i}}{16\pi^2 s} \iint_{-\infty}^0 \mathrm{d}t_1 \, \mathrm{d}t_2 A^{\mathrm{B}}(s,t_1) \, A^{\mathrm{B}}(s,t_2) \frac{\theta(-\lambda)}{(-\lambda(t,t_1,t_2))^{\frac{1}{2}}} \tag{8.4.28}$$

This would agree with (8.4.1), with $N = 1$, if we were to take Regge poles instead of (8.4.21) as the Born approximation, which shows that the precise form of the exchange does not really matter provided the approximation (8.4.12) remains valid. In fact it can be shown (Tiktopoulos and Trieman 1970) that if the particle exchanges in fig. 8.20 are replaced by ladders, the leading diagrams are those in which the couplings at the ends of the ladders cross as in fig. 8.19 (*c*), (*e*), rather

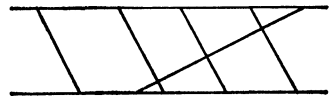

FIG. 8.21 A diagram which violates the eikonal approximation in ϕ^3 theory. Only three propagators are needed to get across the diagram, but there are four along each side.

than the planar fig. 8.19 (b), (d) as one would expect from section 8.2. So the eikonal series (8.2.24) can be regarded as the sum of the Regge cuts due to any number of Reggeons with their couplings 'nested'.

There must, however, be doubt about the applicability of these results to hadronic physics. First they are not actually true in ϕ^3 field theory because the approximation (8.4.12) is invalid. For example, fig. 8.21 has a d-line of length 3 and hence $\sim s^{-3}$. But in the eikonal approximation we suppress the possibility of large momenta travelling across the diagram, because the momentum should mainly travel along the sides, which involves 4 propagators, and hence in this approximation fig. 8.21 $\sim s^{-4}$. So this diagram would violate the eikonal approximation in ϕ^3 theory. However, we have seen in chapter 6 that experimentally momentum transfers are cut off exponentially, so in this respect the approximate version of the field theory seems more realistic than the theory itself. Models with elementary vector meson exchanges have also been examined (Cheng and Wu 1969, 1970). In this case the s-dependence of the exchanged propagators (see (2.6.10)) ensures the validity of the eikonal approximation without a cut-off, but it also means that the Reggeons lie above 1 for all t. We shall discuss this further in the next section.

Fig. 8.19 includes only one set of relevant graphs. In the previous section we mentioned the necessary for iterating the ladders in t as well as s (as in fig. 8.16) to be compatible with t-channel unitarity. There are also more complicated diagrams like fig. 8.22 (called 'checkerboard' diagrams), in which the Reggeons interact during the exchange, which seem to violate the eikonal result (Blankenbecler and Fried 1973, Swift 1975), and diagrams (of which the diffraction diagram fig. 8.18 is an example) in which the leading particle fragments and recombines. Quite apart from the difficulties of including these effects, there is also the usual worry as to whether they are not already partially included (implicitly) as re-normalization corrections to simpler diagrams. This is a fundamental problem with any field-theoretic model. (For a review see Blankenbecler, Fulco and Sugar 1974).

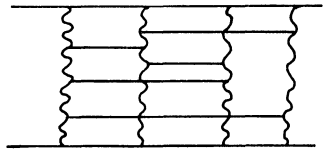

FIG. 8.22 An example of a 'checkerboard' diagram in which the Reggeons interact during the exchange.

In spite of these reservations, the eikonal model offers several advantages. First it ensures satisfaction of s-channel unitarity bounds (in analogy with section 1.14). Secondly it is easily generalized to include different types of Reggeons, and different helicity amplitudes. And thirdly the model is comparatively easy to evaluate. To demonstrate this it is convenient to start from the s-channel partial-wave series for an elastic-scattering helicity amplitude, (4.4.9),

$$A_{Hs}(s,t) = 16\pi \sum_{J=M}^{\infty} (2J+1)\, A_{HJ}(s)\, d^J_{\mu\mu'}(z_s) \tag{8.4.29}$$

At high energies and small angles, $s \gg t$, and large J (Durand and Chiu 1965),

$$d^J_{\mu\mu'}(z_s) \approx J_n((J+\tfrac{1}{2})\,\theta_s), \quad n \equiv |\mu - \mu'| \tag{8.4.30}$$

and

$$\cos\theta_s \equiv z_s \approx 1 + \frac{t}{2q_s^2}, \quad \text{so} \quad \theta_s \approx \left(\frac{-t}{q_s^2}\right)^{\frac{1}{2}} \tag{8.4.31}$$

The classical impact parameter b (fig. 8.23) for a particle passing the target with angular momentum J is given by

$$J = q_s b - \tfrac{1}{2} \tag{8.4.32}$$

(the $\frac{1}{2}$ is arbitrary since we are working with large J) so we can replace $\sum_J$ by $\int_0^\infty q_s\, db$ and hence (8.4.29) becomes

$$A_{H_s}(s,t) = 16\pi \int_0^\infty q_s\, db\, 2q_s b\, A_{HJ}(s)\, J_n(b\sqrt{-t}) \tag{8.4.33}$$

We then express the elastic partial-wave amplitude in unitary form in terms of the phase shift (2.2.10)

$$A_{HJ}(s) = \frac{e^{2i\delta_{HJ}(s)} - 1}{2i\rho(s)} \tag{8.4.34}$$

and define the eikonal phase $\chi_H(s,b)$ in terms of this phase shift by

$$\chi_H(s,b) = 2\delta_{HJ}(s) \tag{8.4.35}$$

https://doi.org/10.1017/9781009403269.009 Published online by Cambridge University Press

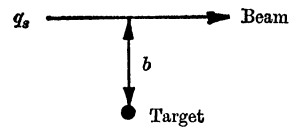

FIG. 8.23 Classical beam, momentum q_s, passing target at impact parameter b has angular momentum $J = q_s b$.

using (8.4.32). This gives the impact parameter amplitude

$$A_H(s,b) = \frac{e^{i\chi_H(s,b)} - 1}{2i\rho(s)} \underset{s\to\infty}{\to} \frac{e^{i\chi_H(s,b)} - 1}{2i} \tag{8.4.36}$$

Physically this replacement means that we are supposing that each part of the wave front of the incident beam passes through the target with its impact parameter unchanged, only its phase being altered. So at high energies conservation of J is replaced by conservation of b through (8.4.23). This corresponds to the derivation in section 1.14. Then (putting $q_s \to \frac{1}{2}\sqrt{s}$)

$$\begin{aligned} A_{H_s}(s,t) &= 8\pi s \int_0^\infty b\,db A_H(s,b) J_n(b\sqrt{-t}) \\ &= 8\pi s \int_0^\infty b\,db \frac{e^{i\chi_H(s,b)} - 1}{2i} J_n(b\sqrt{-t}) \end{aligned} \tag{8.4.37}$$

which agrees with (8.4.21) for the non-flip amplitude, $n = 0$, if we define the eikonal function in terms of the Regge pole exchange Born approximation to the helicity amplitude (like (8.4.20))

$$\chi_H(s,b) = \chi_H^{\mathrm{R}}(s,b) \equiv \frac{1}{8\pi s} \int_{-\infty}^0 dt J_n(b\sqrt{-t})\, A_{H_s}^{\mathrm{R}}(s,t) \tag{8.4.38}$$

Expanding the exponential in (8.4.37) gives us the series of cuts produced by R exchange, i.e. $\mathrm{R} + \mathrm{R} \otimes \mathrm{R} + \mathrm{R} \otimes \mathrm{R} \otimes \mathrm{R} + \ldots$. Since we want to sum over intermediate-state helicities a matrix product of the χ's in helicity space is implied.

For an inelastic process we can invoke the so-called 'distorted wave Born approximation' (see for example Newton (1966)), and replace (8.4.36) by

$$A_H(s,b) = \chi_H^{\mathrm{R}}(s,b)\, e^{i\chi_H^{\mathrm{el}}(s,b)} = \chi_H^{\mathrm{R}} + i\chi_H^{\mathrm{R}}\chi_H^{\mathrm{el}} + \ldots \tag{8.4.39}$$

which obviously corresponds, up to second order, to the absorptive prescription (8.4.4) if we use P for the elastic amplitude. So combining (8.4.39) and (8.3.36) the eikonal/absorption prescription for a Regge

https://doi.org/10.1017/9781009403269.009 Published online by Cambridge University Press

cut involving the exchange of n_1 Reggeons R_1, n_2 of R_2, etc. is

$$A^{c}_{H_s}(s,t) = -i4\pi s \int_0^\infty b\,db\,J_n(b\sqrt{-t})\frac{(i\chi^{R_1}_H)^{n_1}}{n_1!}\frac{(i\chi^{R_2}_H)^{n_2}}{n_2!}\cdots \tag{8.4.40}$$

where each χ is calculated according to (8.4.38), and we must sum over intermediate-state helicities.

It may seem surprising that we have chosen to evaluate the cut contributions in s-channel helicity amplitudes, but in fact this is easiest because the cuts involve s-channel unitarization.

We explore some of the properties of (8.4.40) in the next section.

8.5 Evaluation of Regge cut amplitudes

The expression (8.4.40) is readily evaluated provided the Regge poles are expressed sufficiently simply. If we take a linear trajectory, $\alpha(t) = \alpha^0 + \alpha' t$, and an exponential residue, $\gamma(t) = Ge^{at}$, with the phase (6.8.15), we have for the Regge pole amplitude

$$A^{R}_{H_s}(s,t) = -x(-t)^{n/2}\left(\frac{s}{s_0}\right)^{\alpha^0} e^{-i\pi\alpha^0/2} G e^{ct} \tag{8.5.1}$$

where $x \equiv 1/-i$ for $\mathscr{S} = \pm 1$, and

$$c \equiv a + \alpha'\left(\log\left(\frac{s}{s_0}\right) - i\frac{\pi}{2}\right) \tag{8.5.2}$$

When substituted in (8.4.38) this gives

$$\chi^{R}_{H_s}(s,b) = \frac{-xG(s/s_0)^{\alpha^0} e^{-i\pi\alpha^0/2}}{8\pi s}\int_{-\infty}^{0} dt\,J_n(b\sqrt{-t})\,(-t)^{n/2} e^{ct} \tag{8.5.3}$$

which is evaluated using the result

$$\int_{-\infty}^{0} e^{ct}(-t)^{(n/2)+m} J_n(b\sqrt{-t})\,dt = \left(\frac{b}{2}\right)^n\left(-\frac{\partial}{\partial c}\right)^m\left(\frac{e^{-b^2/4c}}{c^{n+1}}\right) \tag{8.5.4}$$

This may be obtained from Magnus and Oberhettinger (1949, p. 131) when it is realized that multiplying the integrand by t is equivalent to differentiating it with respect to $-c$. So

$$\chi^{R}_{H_s}(s,b) = \frac{-xG(s/s_0)^{\alpha^0} e^{i\pi\alpha^0/2}}{8\pi s}\left(\frac{b}{2c}\right)^n \frac{e^{-b^2/4c}}{c} \tag{8.5.5}$$

This expression gives the impact parameter profile of a Regge pole. Except for non-flip amplitudes ($n = 0$) it must vanish at $b = 0$, and

all the amplitudes are Gaussian in b for large b (because of the assumed exponential t dependence), the width of the profile, given by c, increasing with $\log s$. This accords with our discussion in section 6.8*e*.

Such expressions are substituted in (8.4.40) for each Reggeon, and the integral may be evaluated using (8.5.4) by interchanging b and $\sqrt{-t}$, i.e.

$$\int_0^\infty \mathrm{e}^{-b^2/4c}(b^2)^{(n/2)+m}J_n(b\sqrt{-t})\,b\,\mathrm{d}b = (-t)^{n/2}\left(-4c^2\frac{\partial}{\partial c}\right)^m[(2c)^{n+1}\mathrm{e}^{ct}] \tag{8.5.6}$$

Thus specializing to $n = 0$ we obtain for the $\mathrm{R}_1 \otimes \mathrm{R}_2$ cut

$$A^{c_2}_{H_s}(s,t) = \frac{\mathrm{i}}{8\pi s}\frac{x_1G_1x_2G_2}{c_1+c_2}\left(\frac{s}{s_0}\right)^{\alpha_1{}^0+\alpha_2{}^0}\mathrm{e}^{-(\mathrm{i}\pi/2)(\alpha_1{}^0+\alpha_2{}^0)}\,\mathrm{e}^{[c_1c_2/(c_1+c_2)]t} \tag{8.5.7}$$

so we see that the cut will have a flatter t dependence than the pole, and its impact parameter profile will be

$$\sim \mathrm{e}^{-(b^2/4)[(c_1+c_2)/c_1c_2]} \tag{8.5.8}$$

which has a shorter range than the pole (8.5.5).

Now for $\log(s/s_0) \gg a/\alpha'$ (~ 4 typically)

$$\frac{c_1c_2}{c_1+c_2} \to \frac{\alpha_1'\alpha_2'}{\alpha_1'+\alpha_2'}\left(\log\left(\frac{s}{s_0}\right) - \frac{\mathrm{i}\pi}{2}\right)$$

and so

$$A^{c_2}_{H_s}(s,t) \to -\frac{G_1G_2}{8\pi s_0}\frac{(s/s_0)^{\alpha_c(t)}x_1x_2\,\mathrm{e}^{-(\mathrm{i}\pi/2)\alpha_c(t)}}{a_1+a_2+(\alpha_1'+\alpha_2')(\log s/s_0 - \mathrm{i}\pi/2)} \sim \frac{s^{\alpha_c(t)}}{\log s} \tag{8.5.9}$$

where
$$\alpha_c(t) \equiv \alpha_1^0+\alpha_2^0-1+\left(\frac{\alpha_1'\alpha_2'}{\alpha_1'+\alpha_2'}\right)t \tag{8.5.10}$$

which agrees with (8.2.17) and (8.3.24) for the position of the cut. It also gives the signature factor $x_1x_2\mathrm{e}^{-\mathrm{i}\pi\alpha_c/2}$ which corresponds to the product of the signatures of the two poles as in (8.3.28). But the presence of $(\log s)^{-1}$ in the asymptotic behaviour indicates that the cut is hard, i.e. has a finite discontinuity at the branch point. As $\log s \to \infty$ the phase of the cut corresponds to its power behaviour (as in section 6.8*f*) but for finite $\log s$ the denominator modifies this phase.

Similarly for n identical Reggeons (8.4.40) with (8.5.5) gives

$$\left.\begin{aligned} A^{c_n}_{H_s}(s,t) &= -\mathrm{i}\frac{[-\mathrm{i}xG(s/s_0)^{\alpha^0}\mathrm{e}^{-\mathrm{i}\pi\alpha^0/2}]^n}{(8\pi cs)^{n-1}}\frac{\mathrm{e}^{ct/n}}{nn!} \\ &\to \frac{(xG)^n}{(8\pi s_0c)^{n-1}}\left(\frac{s}{s_0}\right)^{\alpha_c(t)}\mathrm{e}^{(-\mathrm{i}\pi/2)\alpha_c(t)} \sim \frac{s^{\alpha_c(t)}}{(\log s)^n} \\ \alpha_c(t) &\equiv n\alpha^0-(n-1)+\frac{\alpha'}{n}t \end{aligned}\right\} \tag{8.5.11}$$

https://doi.org/10.1017/9781009403269.009 Published online by Cambridge University Press

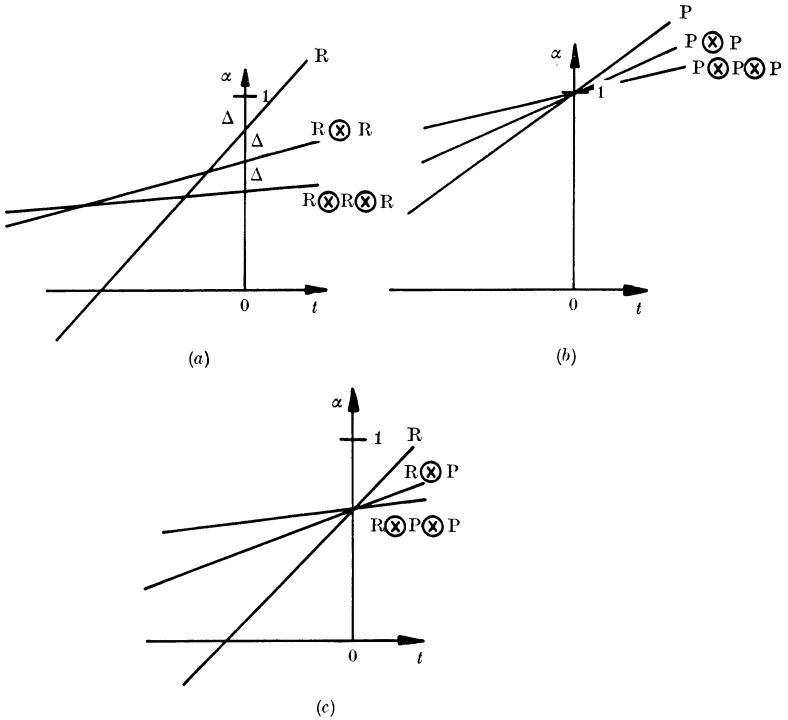

FIG. 8.24 (*a*) Regge trajectory R, and R⊗R, R⊗R⊗R cuts. $\Delta \equiv (1-\alpha^0)$ gives the spacing of successive cuts at $t = 0$, but the higher order cuts are flatter. (*b*) Pomeron cuts converging on $\alpha = 1$ at $t = 0$. (*c*) Reggeon R and the sequence of R⊗P, R⊗P⊗P cuts which converge on α_R^0 at $t = 0$.

which again agrees with (8.2.17) and (8.3.24), and gives

$$A(J,t) \sim (J-\alpha_c(t))^{n-1}$$

as $J \to \alpha_c$. The positions of such cuts are shown in fig. 8.24.

The factor $(-t)^{\frac{1}{2}|\mu-\mu'|}$ in (8.5.6) ensures that cuts of all orders have the correct helicity-flip factor, as long as it is present in the input poles. However, if the poles also have evasive t factors (see section 6.5) cuts generated by these poles will not usually contain these additional factors. This is because the cuts do not have a definite t-channel parity, and so it is natural for them to conspire, not evade.

Combining these results we can write a general expression for an n-Reggeon cut

$$A^c_{H_s}(s,t) = (-t)^{\frac{1}{2}|\mu-\mu'|} F(t) \left(\frac{s}{s_0}\right)^{\alpha_c(t)} e^{(i\pi/2)\alpha_c(t)} \left(\log\left(\frac{s}{s_0}\right) + d\right)^{-n+1} \begin{Bmatrix} 1 \\ -i \end{Bmatrix} \tag{8.5.12}$$

for $\mathscr{S}_c \equiv \prod_{i=1}^{n} \mathscr{S}_i = \pm 1$, where $\alpha_c(t)$ is given by (8.3.24), $F(t)$ is free of kinematical singularities, and d is a constant. The eikonal/absorption prescription gives $F(t)$ and d in the approximation that all the coupling functions $N(t, t_1, t_2, \ldots, t_n) = 1$.

8.6 Pomeron cuts and absorption

Since the Pomeron has $\alpha_P(0) \approx 1$, the cuts generated by Pomeron exchange have rather special properties. Thus if

$$\alpha_P(t) = 1 + \alpha'_P t \tag{8.6.1}$$

the exchange of n Pomerons gives a branch point at

$$\alpha_{c_n}(t) = 1 + \frac{\alpha'_P}{n} t \tag{8.6.2}$$

from (8.3.27). Hence all these cuts coincide at $t = 0$, and since the higher order cuts are flatter they will be above the lower order cuts for $t < 0$, as shown in fig. 8.24(*b*). Similarly from (8.5.10) an R ⊗ P cut will be at

$$\alpha_{c_2}(t) = \alpha^0_R + \left(\frac{\alpha'_R \alpha'_P}{\alpha'_R + \alpha'_P}\right) t \tag{8.6.3}$$

and an R ⊗ $(P)^n$ cut will be at

$$\alpha_c(t) = \alpha^0_R + \left(\frac{\alpha'_R (\alpha'_P)^n}{\alpha'_R + n\alpha'_P}\right) t \tag{8.6.4}$$

so all the cuts coincide with $\alpha_R(t)$ at $t = 0$ and lie above it for $t < 0$ (fig. 8.24(*c*)).

This coincidence of the P pole and its cuts at $t = 0$ means that successive terms in the sum over all numbers of P exchanges differ only by powers of $(\log s)^{-1}$, not powers of s. Hence the re-normalization and unitarity problems mentioned in section 8.3 seem much more severe for Pomerons than for other trajectories. Indeed we shall find in sections 10.8 and 11.7 that naïve iteration of P exchange in t would give a leading behaviour which violates the Froissart bound (that is $A(s, t = 0) \leqslant s \log^2 s$) so that pole dominance, even at $t = 0$, does not seem to be self-consistent. So it is clear that iteration in s, giving 'absorption' of P exchange, must also be important, but unfortunately a proper unitarization in both s and t is beyond our competence. The Reggeon field theory mentioned in section 8.3 suggests that eventually $A(s, t = 0) \sim s(\log s)^\nu$ (where $\nu \approx \frac{1}{6}$ to the first approximation: see

https://doi.org/10.1017/9781009403269.009 Published online by Cambridge University Press

Abarbanel *et al.* (1975)), but it only explicitly takes into account t-channel unitarity, and compatibility with s-channel unitarity is not obvious.

If the leading J-plane singularity is to be self-consistent, it should reproduce itself when inserted in (8.3.24). Obviously linear forms cannot do this, but if one takes (Schwarz 1967)

$$\alpha(t) = 1 \pm i\alpha'\sqrt{-t}\ , \quad \alpha' \text{ constant} \tag{8.6.5}$$

then
$$\alpha_{c_n}(t) \equiv \max\left\{\sum_{i=1}^{n} \alpha(t_i) - n + 1\right\} = \alpha(t) \quad \text{for any } n, \tag{8.6.6}$$

with
$$\sum_{i=1}^{n} \sqrt{-t_i} = \sqrt{t}\ . \tag{8.6.7}$$

So the poles are complex for $t < 0$, but there is no violation of Mandelstam analyticity because the two poles have equal and opposite imaginary parts (see section 3.2). Indeed it generally happens that when poles and cuts collide unitarity requires the trajectories to be complex (see Zachariasen 1971). The fact that $\mathrm{Im}\{\alpha\} \neq 0$ for $t < 0$ gives $s^{\alpha(t)} = s^{\alpha_R(t)} e^{i\alpha_I(t)\log s}$ (where $\alpha_{R,I}$ are the real and imaginary parts of α respectively) and so the phase–energy relation (8.6.14) will not hold, and the Regge power behaviour will be modulated by oscillations in $\log s$. There has so far been no sign of these effects, and the effective trajectories of fig. 6.6 all seem to be linear in t. It may be of course that we need $\log s \gg a/\alpha'$ to observe such effects, in which case it will be some time before they can be verified.

With $\alpha_P(0) = 1$, $x = 1$, we obtain for the sum of all P exchanges, from (8.5.11),

$$A_{H_s}(s,t) = \sum_{n=1}^{\infty} A^{c_n}(s,t) = \sum_{n=1}^{\infty} -i\frac{[-G(s/s_0)]^n}{(8\pi cs)^{n-1}} \frac{e^{ct/n}}{nn!} \tag{8.6.8}$$

which, setting $s_0 = 1$, gives

$$\sigma^{\mathrm{tot}}_{12\to\mathrm{all}}(s) = \frac{1}{s}\mathrm{Im}\{A^{12\to12}(s,0)\} = G - \frac{G^2}{32\pi c} + \frac{G^3}{1152\pi^2c^2} - \ldots$$
$$\to G\left(1 - \frac{G}{32\pi\alpha'\log s} + \ldots\right) \tag{8.6.9}$$

so if we assume that the series converges (which may be false) we predict that $\sigma^{\mathrm{tot}}(s) \to$ constant logarithmically from below. This rise of σ^{tot} depends crucially on the sign of the cut being that of the eikonal/absorption model and the Reggeon calculus, not the AFS sign, which with our pure imaginary P amplitude (at $t = 0$) would give

a positive second term. Unfortunately, the magnitude of the cut term in (8.6.9) is insufficient to account for the rise of $\sigma^{\text{tot}}(\text{pp})$ (fig. 6.4) as it stands. However, if we use the freedom suggested by (8.3.8) and (8.2.37) to multiply the cut strength by an arbitrary factor N^2, we can choose N to fit the data. But this makes the cuts very strong, and the convergence of the series even more doubtful (see section 8.7*a* below).

Of course if $\alpha_{\text{P}}(0) < 1$ the pole and cuts are separated by a finite amount $\Delta \equiv (1-\alpha_{\text{P}}(0))$ at $t = 0$ (fig. 8.24*a*), but this makes the observed rise of σ^{tot} hard to understand. In fact fig. 6.6 suggests that $\alpha_{\text{P}}(0) > 1$, but this can only be compatible with the Froissart bound (2.4.9) if unitarization produces strong cancelling cuts. We can see how this works as follows. If $\alpha_{\text{P}}(0) > 1$, then from (8.5.5) with $n = 0$,

$$\chi_H^{\text{P}}(s,b) = -\frac{G_{\text{P}}(s/s_0)^{(\alpha_{\text{P}}{}^0-1)}\,\mathrm{e}^{-\mathrm{i}\pi\alpha_{\text{P}}{}^0/2}\,\mathrm{e}^{-b^2/4c_{\text{P}}}}{8\pi s_0 c_{\text{P}}}$$

$$= -\frac{G_{\text{P}}}{8\pi s_0 c_{\text{P}}}\,\mathrm{e}^{-\mathrm{i}\pi\alpha_{\text{P}}{}^0/2}\,\mathrm{e}^{[-b^2/4c_{\text{P}}+(\alpha_{\text{P}}{}^0-1)\log(s/s_0)]} \tag{8.6.10}$$

so if
$$b^2 < b_0^2 \equiv 4(\alpha_P^0 - 1)\,\alpha_P' \log^2\left(\frac{s}{s_0}\right) \tag{8.6.11}$$

then
$$\chi_H^{\text{P}}(s,b) \to 0 \qquad \text{as } s \to \infty,$$

but for $b^2 > b_0^2$
$$\chi_H^{\text{P}}(s,b) \to 0$$

So from (8.4.36)
$$A_H(s,b) \to \tfrac{1}{2}\mathrm{i}, \quad b^2 < b_0^2$$
$$\to 0, \quad b^2 > b_0^2 \tag{8.6.12}$$

This is like complete absorption on a black disk of radius b_0. Now $J_0(b\sqrt{-t}) \to 1$ for $t \to 0$, so from (8.4.37)

$$\text{Im}\{A_{H_s}(s,0)\} = 8\pi s \int_0^\infty b\,\mathrm{d}b\,\text{Im}\{A_H(s,b)\} \to 4\pi s \int_0^{b_0} b\,\mathrm{d}b = 2\pi s b_0^2 \tag{8.6.13}$$

and so
$$\sigma_{12}^{\text{tot}}(s) \to 8\pi\alpha_{\text{P}}'(\alpha_{\text{P}}^0 - 1)\log^2\left(\frac{s}{s_0}\right) \tag{8.6.14}$$

in accord with the Froissart bound. However, with the numbers of fig. 6.6, $\alpha_{\text{P}}' \approx 0.25\,\text{GeV}^{-2}$, $\alpha_{\text{P}}^0 \approx 1.07$, this gives

$$\sigma_{12}^{\text{tot}}(s) \to 3.6\log^2\left(\frac{s}{s_0}\right)\text{mb}$$

which with $s_0 = 1$ is much in excess of current measurements ($\sigma^{\text{tot}}(\text{pp}) \approx 44\,\text{mb}$ for $\log s \approx 8$ at ISR). So if this model is correct very

https://doi.org/10.1017/9781009403269.009 Published online by Cambridge University Press

much higher energies will have to be achieved before the observed pole-like behaviour $\sigma^{\text{tot}}(\text{pp}) \sim 27 s^{0.07}$ mb turns into the $\log^2 s$ asymptotic behaviour. If more complex diagrams than fig. 8.19, like fig. 8.22, are permitted, then $\alpha_{\text{P}}(0) > 1$ gives a grey disk instead ($\text{Im}\{A(s,b)\} < \frac{1}{2}$) but the main conclusions are unaltered; see Bronzan (1974), Cardy (1974*a*).

It is evident from (8.4.40) that for inelastic scattering, where P cannot be exchanged, in addition to the dominant R exchange there will be a sequence of $\text{R} \otimes (\text{P})^n$ cuts which should dominate for $t < 0$, $s \to \infty$. Thus if we use (8.5.1) for R and take $\alpha_{\text{P}}(0) = 1$, the $\text{R} \otimes \text{P}$ cut from (8.5.7) will be

$$A_{H_s}^{\text{R}\otimes\text{P}}(s,t) = \frac{\lambda x_{\text{R}} G_{\text{R}} G_{\text{P}}}{8\pi a_0} \left(\frac{s}{s_0}\right)^{\alpha_{\text{R}}{}^0} \frac{e^{-i\pi\alpha_{\text{R}}{}^0/2}}{c_{\text{R}} + c_{\text{P}}} e^{c_{\text{R}} c_{\text{P}}/(c_{\text{R}}+c_{\text{P}})t} \quad (8.6.15)$$

where λ is the enhancement factor.

This has the same asymptotic phase as the pole (8.5.1) but the opposite sign at $t = 0$, and for t near zero where $\alpha_c \approx \alpha_{\text{R}}$. Also the t dependence of the cut is shallower than that of the pole, so even if the pole dominates the cut at $t = 0$, there will be a cancellation (destructive interference) between cut and pole for some $t < 0$, as shown in fig. 8.25. Approximately (neglecting higher order cuts),

$$A_{H_s}(s,t) \approx A^{\text{R}} + A^{\text{R}\otimes\text{P}} = -x_{\text{R}} G_{\text{R}} \left(\frac{s}{s_0}\right)^{\alpha_{\text{R}}{}^0} e^{-i\pi\alpha_{\text{R}}{}^0/2} \times \left(e^{c_{\text{R}} t} - \frac{\lambda G_{\text{P}}}{8\pi s_0} e^{[c_{\text{R}} c_{\text{P}}/(c_{\text{R}}+c_{\text{P}})]t}\right) \quad (8.6.16)$$

and for small $|t|$, where the phase of the pole and cut are similar, there will be an almost simultaneous zero in $\text{Re}\{A_{H_s}\}$ and $\text{Im}\{A_{H_s}\}$ and so there may be a dip in $\text{d}\sigma/\text{d}t$. As we shall see in the next section, this may provide an explanation for some of the dips discussed in section 6.8*k*.

It is interesting to examine the impact parameter structure of this amplitude. From (8.4.39) we can write

$$\begin{aligned} A_H(s,b) &\approx \chi_H^{\text{R}}(s,b) + i\lambda \chi_H^{\text{R}}(s,b)\, \chi_H^{\text{P}}(s,b) \\ &= \chi_H^{\text{R}}(s,b)\,(1 + i\lambda \chi_H^{\text{P}}(s,b)) \end{aligned}$$

which since P is almost pure imaginary becomes

$$\approx \chi_H^{\text{R}}(s,b)\,(1 - \lambda |\chi_H^{\text{P}}(s,b)|) \quad (8.6.17)$$

which is exhibited in fig. 8.26, from which it is seen that the effect of

https://doi.org/10.1017/9781009403269.009 Published online by Cambridge University Press

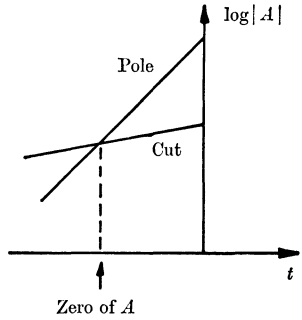

FIG. 8.25 Pole and cut magnitudes as a function of t at fixed s. The different exponential t dependences in (8.6.16) result in an approximate zero where the pole and cut magnitudes are the same (neglecting the phase difference which is small for small $|t|$).

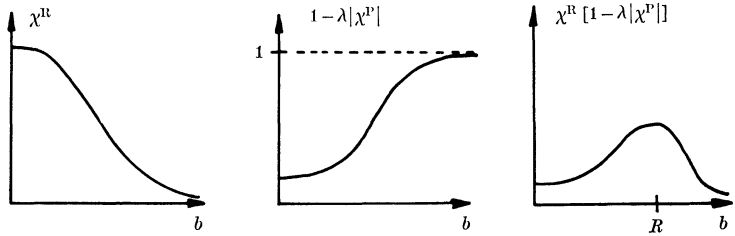

FIG. 8.26 (*a*) The Gaussian impact-parameter profile of a Regge pole from (8.5.5) with $n = 0$. (*b*) The absorption S-matrix. (*c*) The impact profile of the absorbed amplitude (8.6.17) showing the reduction of the amplitude at small b, i.e. low J. The resulting peak is at $b = R \approx 1$ fm.

absorption is to reduce the Reggeon amplitude at small b through the destructive effect of the shorter range cut. By a suitable choice of λ we can eliminate small-b scattering (complete absorption) so that the predominant part of the scattering amplitude is at $b \approx 1$ fm, the periphery of the target. For helicity-flip amplitudes the kinematical b^n in (8.5.5) means that the Regge pole amplitude is already fairly peripheral, and the effect of absorption is much smaller in this case.

One can roughly approximate this peripheral profile by a δ-function in b-space at radius R

$$A_H(s,b) \approx \frac{-xG_H}{8\pi s} e^{-i\pi\alpha/2} \left(\frac{s}{s_0}\right)^{\alpha} \frac{1}{R} \delta(b-R) \qquad (8.6.18)$$

where $R = 1$ fm, which when substituted in (8.4.37) gives

$$A_H(s,t) = -xG_H e^{(-i\pi/2)\alpha(t)} \left(\frac{s}{s_0}\right)^{\alpha(t)} J_n(R\sqrt{-t}) \qquad (8.6.19)$$

https://doi.org/10.1017/9781009403269.009 Published online by Cambridge University Press

for the sum of pole and cut. In this approximation we have completely ignored the difference between $\alpha_R(t)$ and $\alpha_c(t)$ in both the power behaviour and phase, and have dropped the $\log s$ factor from the cut. With $R = 1$ fm the first zeros of the Bessel function appear at $-t = 0.2$, 0.55 and 1.2 GeV^2 for $n = 0$, 1, 2, respectively (Henyey *et al.* 1969), positions which correspond to some of the amplitude zeros noted in section 6.8. We shall examine this result further in the next section.

8.7 Regge cut phenomenology

Having established the general features of Regge cut contributions we can now try and discover whether they can make good the deficiencies of Regge poles found in section 6.8.

Once we know the Regge pole trajectories, the positions of the various branch points, and hence the power behaviour and asymptotic phase of the cut contributions, are fixed by (8.3.24). Also the kinematical restrictions on the cuts are very simple for s-channel helicity amplitudes, which we used in (8.5.12). This leaves us with two main problems. First, we need to find $F(t)$ and d in (8.5.12). They are predicted by the eikonal/absorption model, but when we compare (8.4.28) with the Reggeon calculus result (8.3.8) it seems doubtful if the model will be reliable in this respect. If N in (8.3.8) is regarded as an unknown, then so are F and d. Secondly, we cannot be sure at what energy an expression like (8.5.12) becomes applicable. In the various derivations of sections 8.2, 8.3 and 8.4 we have taken only the leading $\log(s/s_0)$ behaviour of each diagram, which suggests that $\log(s/s_0) \gg 1$ is needed, which is seldom achieved in practice. This problem is worst for cuts involving the P where successive terms in the eikonal expansion differ only by $(\log(s/s_0))^{-1}$.

Keeping these uncertainties in mind we can now review some of the difficulties left over from section 6.8.

a. Total cross-sections and elastic scattering

The rising $\sigma^{\text{tot}}(s)$ shown in fig. 6.4 require either $\alpha_P(0) > 1$, which will eventually violate the Froissart bound unless there are cut corrections, or $\alpha_P(0) = 1$ and very strong cuts (see (8.6.9) *et seq.*). Thus for pp scattering we can write

$$\sigma_{pp}^{\text{tot}}(s) = iG_P\left(1 - \frac{\lambda G_P}{32\pi\alpha_P' \log s} + \ldots\right) \tag{8.7.1}$$

https://doi.org/10.1017/9781009403269.009 Published online by Cambridge University Press

where λ is the enhancement factor, and one needs $G_P \approx 85\,\text{mb}$, $\lambda \approx 2$ to fit the data. But the shallower t dependence of the cut means that cut and pole cancel for $|t| \approx 0.5\,\text{GeV}^2$, predicting a dip in $d\sigma/dt$ which is not observed. There does not seem to be any simple way out of this dilemma (see Collins *et al.* 1974). But $\alpha_P(0) \approx 1.07$ fits all the σ^{tot} data perfectly and there does not seem to be any sign at small $|t|$ of the cuts which will eventually be needed to ensure satisfaction of the Froissart bound. But since $\sigma^{tot}(s) = 27s^{0.07}\,\text{mb}$ does not violate the Froissart bound $\sigma^{tot}(s) \leqslant 60\log^2 s\,\text{mb}$ until $s \simeq 10^{75}\,\text{GeV}^2$, this is hardly surprising.

It is possible to explain the dip in $d\sigma/dt(pp)$ at $|t| \approx 1.4\,\text{GeV}^2$ (fig. 8.27(*a*)) as interference between the P and the P $\otimes$ P cut (as in (8.6.16) with R $\to$ P) and the effective trajectory plot (fig. 8.27(*b*)) supports this idea. But since the dip occurs at such large $|t|$ we need a very small λ, $\approx \frac{1}{15}$. Also since the forward peak has $d\sigma/dt \sim e^{12t}$, while for $|t| > 1.4\,d\sigma/dt \sim e^{2t}$, (8.6.16) which gives $A^c \sim e^{c_p t/2}$ will not do. We need to put some t dependence into N in (8.4.1), say $N^2 = \lambda e^{bt}$ with $b < 0$. So if fig. 8.27 is an example of Regge cuts in elastic scattering their properties must be very different from those of the simple eikonal model (Collins *et al.* 1974).

b. The cross-over zero

This zero in the ω and ρ non-flip coupling to nucleons is discussed in section 6.8*l*. The fact that it appears at $|t| \approx 0.15\,\text{GeV}^2$ is just what one might have expected from the destructive interference of the R pole and R $\otimes$ P cut, from (8.6.19) with $n = 0$. Since this zero does not factorize it seems almost inevitable that cuts should provide the explanation, and it certainly seems to vindicate the absorption idea (Henyey *et al.* 1969).

c. Nonsense dips

Table 6.7 shows that the explanation of dips like that in

$$d\sigma/dt(\pi^- p \to \pi^0 n)$$

at $|t| \approx 0.55\,\text{GeV}^2$ as being due to a nonsense zero at $\alpha_\rho(t) = 0$ in A_{+-} is incompatible with factorization. Again the t value is just where (8.6.19) predicts a zero in the $n = 1$ amplitude, so cut–pole interference seems to provide a preferable explanation. There is a difficulty,

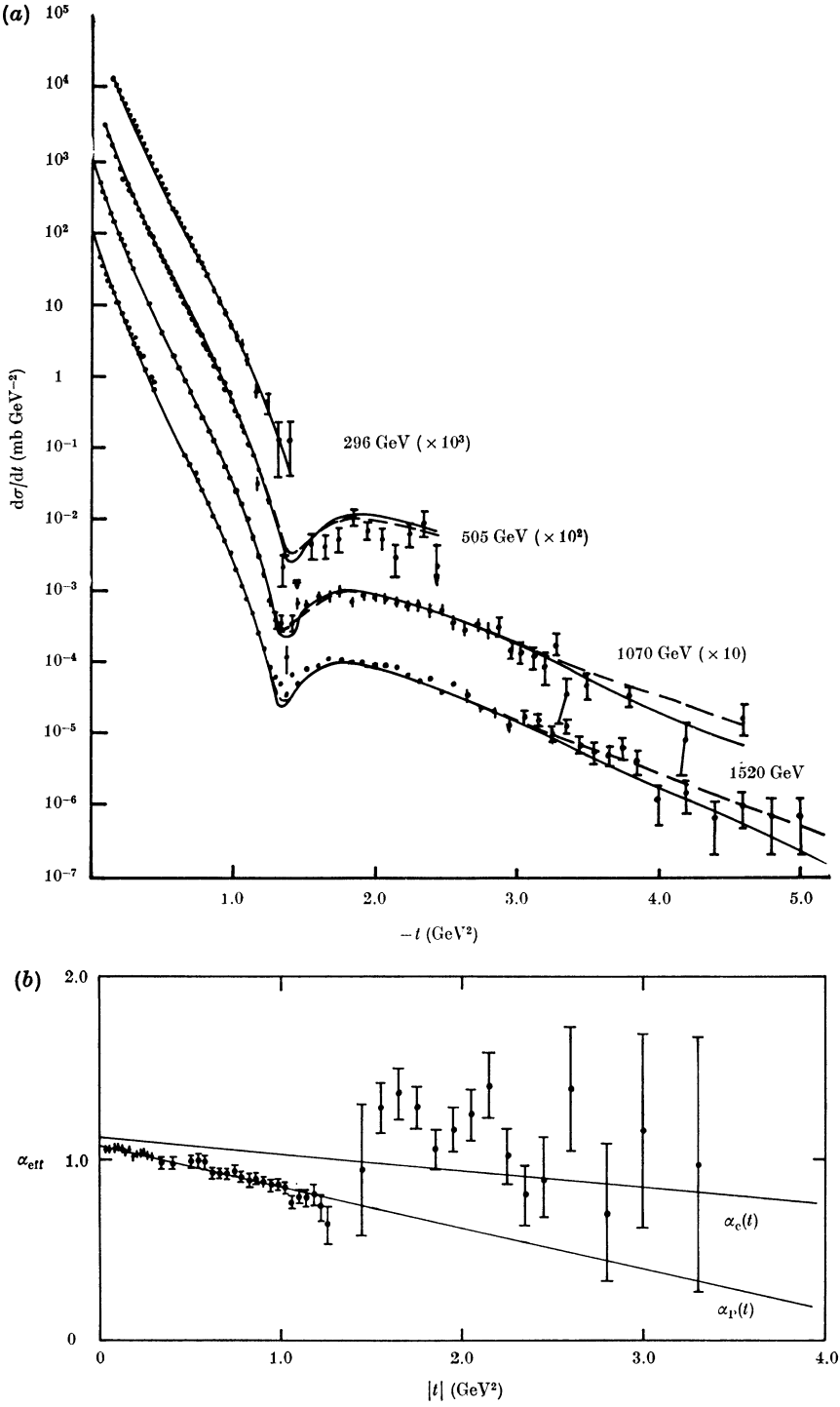

FIG. 8.27 (*a*) Fit $d\sigma/dt$ (pp) data with P and P$\otimes$P cut (from Collins *et al.* 1974). (*b*) The effective trajectory of the data compared with α_P and α_c. The pole dominates for $|t| < 1.4\,\text{GeV}^2$ and the cut for $|t| > 1.4\,\text{GeV}^2$.

https://doi.org/10.1017/9781009403269.009 Published online by Cambridge University Press

however, in that the kinematics of A_2 exchange in $\pi^-p \to \eta n$ are very similar to that of ρ exchange in $\pi^-p \to \pi^0 n$ so one would expect a dip due to cut–pole interference in this case too, but it is not seen. (Since $\alpha_{A_2} = 0$ is a right-signature point we do not expect a nonsense zero.) This could be because A_2 exchange is of shorter range ($m^2_{A_2} > m^2_\rho$) so $c_{A_2} < c_\rho$, and in (8.6.16) the $A_2 + A_2 \otimes P$ dip would appear at larger $|t|$ (Martin and Stevens 1972). Or the absorbing amplitude may contain more than just the imaginary P, in which case the phase difference between ρ and A_2 exchange (due to their different signatures) will produce dips in different places (Hartley and Kane 1973). Since the signature properties are an essential feature of dual models, Harari (1971) has proposed a dual absorption model in which the absorptive prescription (8.6.19) is used only for $\mathrm{Im}\{A\}$, i.e.

$$\mathrm{Im}\{A_{H_s}(s,t)\} = G_H \left(\frac{s}{s_0}\right)^{\alpha(t)} J_n(R\sqrt{-t}) \tag{8.7.2}$$

but the dispersion relations give a real part which depends on the signature (from (6.8.18)), and so

$$A_{H_s}(s,t) = -G_H \left[\frac{e^{-i\pi\alpha} + \mathscr{S}}{\sin \pi\alpha}\right] \left(\frac{s}{s_0}\right)^{\alpha(t)} J_n(R\sqrt{-t}) \tag{8.7.3}$$

which has a zero at $\alpha = 0$ for the $\mathscr{S} = -1$ ρ, but not for the A_2 with $\mathscr{S} = +1$. However, this does not work for K*, K** exchange process, where $\alpha = 0$ for $|t| \approx 0.2\,\mathrm{GeV}^2$ which does not coincide with the $n = 1$ zero of (8.7.3) unless R is increased to about 1.6 fm (Irving, Martin and Barger 1973). So although the absorptive explanation of dips may be right, the nature of the absorption must be fairly complex.

d. Polarization and phases

With a purely imaginary P (8.6.16) gives coincident zeros for $\mathrm{Re}\{A\}$ and $\mathrm{Im}\{A\}$. Thus in $\pi^-p \to \pi^0 n$ the polarization (4.2.22) would have a zero at $|t| \approx 0.15\,\mathrm{GeV}^2$, coincident with cross-over, if the absorptive explanation were the complete answer. This is not observed, and the phase analysis in fig. 6.10 shows that the zero of $\mathrm{Re}\{A_{++}\}$ does not occur until $|t| \approx 0.5\,\mathrm{GeV}^2$, where there appears to be a double zero. These effects can be explained by the absorption model only if the absorbing amplitude has a substantial, t-dependent, real part. The small slope of the P ($\alpha'_P \approx 0.2\,\mathrm{GeV}^{-2}$) provides an insufficient phase change, but if the f is included, so that we have $R + (P + f) \otimes R$

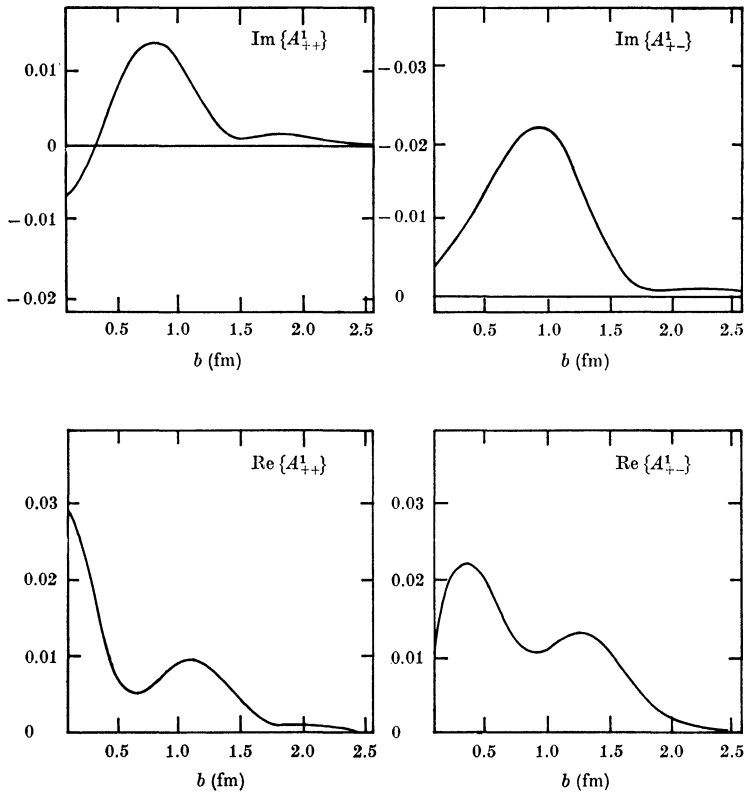

FIG. 8.28 The impact parameter amplitudes for $I_t = 1$ πN elastic scattering at 6 GeV, corresponding to fig. 6.10, from Halzen and Michael (1971).

instead, fairly satisfactory fits can be obtained (Collins and Swetman 1972). Other, more *ad hoc*, modifications of the phase have also been proposed (Hartley and Kane 1973). But whether this sort of approach is correct given that, as discussed in section 6.8*m*, only $\mathrm{Im}\{A_{++}\}$ is different from what we expect from a nonsense-choosing ρ pole, is not certain. The impact parameter decomposition (8.4.38) of the amplitude in fig. 6.10 gives fig. 8.28. Since a pole without nonsense factors gives fig. 8.26 (*a*), it is clear that, for small b, $\mathrm{Im}\{A_{++}(s, b)\}$ is not just being absorbed but over-absorbed (i.e. its sign is reversed) which conflicts with any simple physical interpretation of what absorption is supposed to mean.

https://doi.org/10.1017/9781009403269.009 Published online by Cambridge University Press

e. Exchange degeneracy and line-reversal breaking

In section 6.8*h* we noted that though exchange degeneracy demands equality of processes related by line reversal, one having the real phase (6.8.22) and the other the rotating phase (6.8.21), in practice this was often not so. It might be hoped that inclusion of cuts would correct this defect, but in fact they seem to make matters worse. This is because in processes with a rotating phase the destructive effect between pole and cut is not as great as for processes with a real phase (which gives a real cut if the absorbing amplitude is purely imaginary). So rotating phase cross-sections should be bigger than real cross-sections, whereas experimentally the reverse seems to be true. The problem is confused by the fact that at least for the ρ and A_2 trajectories of figs. 6.6 exchange degeneracy seems to be broken, and there may be important contributions from lower trajectories, R ⊗ f cuts, etc., at lower energies, quite apart from uncertainties in the data normalization (see for example Lai and Louie 1970, Michael 1969*a*, Irving *et al.* 1971).

f. Conspiracies

In section 6.8*j* we found that (unless there are conspiracies) the factorization and parity restrictions may introduce extra kinematical factors into Regge pole amplitudes, causing them to vanish at $t = 0$. This is particularly important for π exchange in processes such as $\gamma p \to \pi^+ n$, $\pi p \to \rho p$, $\bar{p}p \to \bar{n}n$ which would have amplitudes like

$$A(s,t) \sim \frac{t}{t-m_\pi^2}, \quad t \to 0 \tag{8.7.4}$$

However, we saw in table 6.6 that in practice spikes often occur. Since cuts are self-conspiring they do not have to vanish at $t = 0$ in non-flip amplitudes, but of course they will not contain the pion pole. But if we take $\pi + \pi \otimes P$, where $\pi \otimes P$ is slowly varying near $t = 0$, we get

$$A(s,t) \sim \frac{t}{t-m^2} - 1 = \frac{m_\pi^2}{t-m_\pi^2} \tag{8.7.5}$$

which has the pion pole but no evasive t factor. The effect of the cut is to absorb away the S-wave contribution of the pion pole (S-wave because it is independent of t and hence z_s). This is sometimes called the Williams model (Williams 1970) or 'poor man's absorption'. This

procedure can account for the forward structure in the processes listed in table 6.6. At $t = 0$ the amplitude is purely cut (no pole), so the magnitude of the cut is unambiguously determined, and it is very large. In $\gamma p \to \pi^+ n$, for example, a model like (8.6.17) needs $\lambda \approx 3$ (Kane *et al.* 1970).

g. Shrinkage and pole-dominated cuts

Since cuts are flatter in t than poles (fig. 8.24) they should become dominant for large s and $|t|$, so one would expect that the amount of shrinkage would decrease, and α_{eff} would become flatter as $|t|$ increases. This does indeed happen in a few cases such as pp elastic scattering (fig. 8.27(*b*)) and photo-production. But these processes are quite atypical since most hadronic inelastic channels like fig. 6.6 show linear α_{eff}, $\alpha' \approx 0.9\,\text{GeV}^{-2}$, out to the largest measured $|t|$. Thus $\pi^- p \to \pi^0 n$ has $\alpha_{\text{eff}} = \alpha_\rho \approx 0.55 + 0.9t$ despite the fact that the $\rho \otimes \text{P}$ cut with

$$\alpha_c(t) \approx \alpha_\rho^0 + \frac{\alpha_\rho' \alpha_P'}{\alpha_\rho' + \alpha_P'} t \approx 0.55 + 0.2t \tag{8.7.6}$$

(see (8.6.3)) is supposed to dominate A_{++} for $|t| > 0.2\,\text{GeV}^2$, and A_{+-} for $|t| > 0.55\,\text{GeV}^2$, if the arguments of sections 8.7*b* and *c* are correct. This persistence of a pole-like α_{eff} is extremely puzzling. It may indicate that it is quite wrong to blame the failures of factorization on cuts. But perhaps a more likely explanation is that at current energies the cut contribution does not come mainly from the region of the discontinuity near the branch point as (8.4.1) assumes. One reason for this is probably the necessity for the cut discontinuity to vanish at the branch point (see section 8.3), a feature which is not built into the eikonal/absorption calculation. Another more controversial possibility (Cardy 1974*b*) is that the N's in fig. 8.12 are in fact dominated by poles, so that the leading contribution to the cut is given by fig. 8.14(*a*), and

$$\left.\begin{aligned} A_J(t) &\sim \frac{(J-\alpha_c)^2}{(J-\alpha_R)^2} \log (J-\alpha_c) \\ \Delta_J\{A_J(t)\} &\sim \frac{(J-\alpha_c)^2}{(J-\alpha_R)^2} \end{aligned}\right\} \tag{8.7.7}$$

where $(J-\alpha_R)^{-1}$ is the Reggeon propagator, $\log(J-\alpha_c)$ arises from the cut loop-integration, and $J-\alpha_c$ occurs at each triple-Reggeon vertex to make the discontinuity vanish at $J = \alpha_c$. When (8.7.7) is substituted in (4.6.2) we find that $A(s,t) \sim s^{\alpha_c}(\log s)^{-3}$ as $\log s \to \infty$,

but $A(s,t) \sim s^{\alpha_R}$ for finite $\log s$ because the pole provides the dominant region of the discontinuity. Such a model can certainly be made to fit the data (e.g. Collins and Fitton 1975) but as we have no prescription for calculating the magnitude of the cut discontinuity in terms of the pole parameters there is a good deal of arbitrariness. Also fig. 8.14 (a) suggests that the sum of pole and cut should factorize, which is clearly no good.

h. Exotic exchanges

Because of this uncertainty about the importance of cut contributions it would be very useful to be able to examine amplitudes where no Regge pole can be exchanged, so cuts alone should appear. Clearly $R \otimes P$ cuts are no good because they have the same quantum numbers as R itself, so we must look for $R \otimes R$ exchanges. If $\alpha_R(0) \approx 0.5$ then (8.63) gives $\alpha_{RR}(0) \approx 0$, so we expect a rapid decrease of these cross-sections with energy, $\sim s^{-2}(\log s)^{-2}$.

For example $\pi^-p \to \pi^+\Delta^-$ involves the exchange of 2 units of charge, $I_t = 2$, so the leading exchange should be a $\rho \otimes \rho$ cut. Unfortunately the forward differential cross-section for this process, and many of the other exotic exchange processes listed in table 6.5, have proved too small to measure except close to threshold. Some processes which have been observed are $\pi^-p \to K^+\Sigma^-$ and $K^-p \to \pi^+\Sigma^-$ ($\rho \otimes K^*$ exchange) and $K^-p \to K^+\Xi^-$ ($K^* \otimes K^*$ exchange). There is some evidence that the $\sim s^{-2}$ behaviour is setting in for $s > 5\,\text{GeV}^2$, and that the magnitude of the cut is compatible with estimates using (8.4.1) with $N^2 = \lambda = 1 - 1.5$ (see Phillips 1967, Michael 1969*b*, Quigg 1971). Another measured process is $K^-p \to pK^-$ which requires charge = 2, strange, baryon exchange, so one would expect the leading singularity to be the $K^* \otimes \Delta$ cut, $\sim s^{-3}$, but up to 6 GeV a s^{-10} decrease of $d\sigma/dt$ is found.

If better data on this class of processes can be obtained, it should help to clarify our ideas about cuts considerably.

i. Regge cuts and duality

In section 7.6 we remarked that since amplitude structures such as the cross-over zero in $\text{Im}\{A_{++}(\pi^-p \to \pi^0n)\}$ and the forward peak in $\gamma p \to \pi^+n$, which may be due to cuts, are also present in the FESR average of the s-channel resonances, these resonances must be dual to the sum $R + R \otimes P$ not just R.

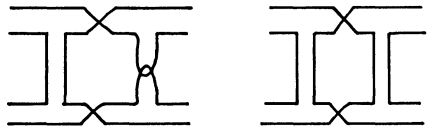

(*a*) (*b*)

FIG. 8.29 Duality diagrams for (*a*) R⊗P cut, (*b*) R⊗R cut in meson–meson scattering.

Duality diagrams for these R ⊗ P cuts can be drawn as in fig. 8.29 (*a*), where we have been careful to include the double-cross structure, so that each quark scatters only once (cf. fig. 8.8 (*c*)). The diagram for an R ⊗ R cut in meson–meson scattering (fig. 8.29 (*b*)) shows that it is dual to the P in the s or u channels. For meson–baryon scattering there is only one R ⊗ R diagram, because the baryon quarks must all travel in the same direction, and this diagram can only be drawn if both the s and u channels are non-exotic, so we can expect R ⊗ R to contribute to the resonances in these channels (in the sense of duality). It also means that there should be no R ⊗ R cuts in a process like $K^-p \to \bar{K}^0 n$ since the λ quark must travel straight across the diagram.

Worden (1973) has shown that the R ⊗ R cuts should cancel in some processes such as $\pi^-p \to \pi^0 n$ because of exchange degeneracy. Briefly his argument may be interpreted as follows. Because of the crosses, and the fact that each signatured Regge pole is the sum of two parts ($\amalg + \mathscr{S}\ \amalg\!\times\!\amalg$), the f ⊗ ρ and ω ⊗ A_2 cuts will cancel if f, ω, ρ and A_2 are exchange degenerate in both their trajectories and their couplings. Although the duality diagrams apply only to Im{A}, the phase–energy relation ensures that the cancellation works for Re{A} too. This is rather a disturbing result because, as we mentioned in section 8.7 *d*, many of the phase problems of the R + R ⊗ P absorption model can be solved by the inclusion of R ⊗ f cuts as well. However, since exchange degeneracy is not exact it is not clear how compelling this argument is.

j. Fixed cuts

In addition to the moving Regge cuts there are also fixed cuts whose positions are independent of t. These are the fixed square-root branch points at sense–nonsense points (see section 4.8) with branch cuts running from $J = M - 1$ to $-M$. However, since $d^J_{\lambda\lambda'}(z_t)$ has compensating branch points these cuts do not contribute to the asymptotic

https://doi.org/10.1017/9781009403269.009 Published online by Cambridge University Press

behaviour of the scattering amplitude. It is possible that their presence might permit the existence of fixed poles at nonsense points $J_0 < M-1$, but there is no evidence that they do, and no obvious mechanism exists to ensure that the kinematic cut discontinuity can contain the pole (as Regge cuts do for Gribov–Pomeranchuk fixed poles).

Fixed cuts have also been suggested as a way of coping with the generalized MacDowell symmetry for baryon Regge poles and the absence of parity doublets (see (6.5.13)). Carlitz and Kisslinger (1970) have suggested that scattering amplitudes may have a fixed cut at $J = \alpha^0$ (where $\alpha^0 \equiv \alpha(t=0)$) and that the negative-parity trajectory (say) will move through it on to an unphysical sheet for positive $\sqrt{t}$ so that it will not give any physical poles. For example

$$A^{\eta}_{HJ}(t) = \beta(t)\frac{(\alpha')^{\frac{1}{2}}\sqrt{t}+\eta(J-\alpha^0)^{\frac{1}{2}}}{J-\alpha^0-\alpha' t}\frac{1}{(J-\alpha^0)^{\frac{1}{2}}} \tag{8.7.8}$$

has the pole at $J = \alpha^0+\alpha' t$ and the cut at $J = \alpha^0$, and the constraint (6.5.13) is automatically satisfied. But in the $\eta = -1$ amplitude there are no poles for positive t. However, such models have not proved very satisfactory phenomenologically (Halzen *et al.* 1970). More recently it has been shown by Savit and Bartels (1975) that similar cuts occur in Reggeon field theory due to the interaction of the fermion with Pomerons. These cuts not only swallow up the unwanted wrong-parity states, but also turn a bare trajectory $\sim \sqrt{t}$ into a re-normalized trajectory approximately $\sim t$. This may explain figs. 5.6.

The rather sad conclusion to be drawn from this whole section is that despite the development of various models which have improved our understanding of Regge cuts and unitarity in the J plane, and despite the partial success of absorption ideas in correcting some of the worst phenomenological defects of Regge poles, we still do not really know how important cuts are. This is probably because we can expect Regge poles to be useful for all $s/s_0 \gg 1$, but cut theories are only really applicable for $\log(s/s_0) \gg 1$ and even at CERN-ISR the maximum value of $\log s$ is only 8.